

Article

SOX17 enables immune evasion of early colorectal adenomas and cancers

<https://doi.org/10.1038/s41586-024-07135-3>

Received: 23 March 2023

Accepted: 30 January 2024

Published online: 28 February 2024

 Check for updates

Norihiro Goto¹, Peter M. K. Westcott^{1,2,12}, Saori Goto^{1,12}, Shinya Imada¹, Martin S. Taylor³, George Eng^{1,3}, Jonathan Braverman^{1,4}, Vikram Deshpande⁵, Tyler Jacks¹, Judith Agudo^{6,7,8,9,10,13} & Ömer H. Yilmaz^{1,3,5,11,13}

A hallmark of cancer is the avoidance of immune destruction. This process has been primarily investigated in locally advanced or metastatic cancer^{1–3}; however, much less is known about how pre-malignant or early invasive tumours evade immune detection. Here, to understand this process in early colorectal cancers (CRCs), we investigated how naïve colon cancer organoids that were engineered *in vitro* to harbour *Apc*-null, *Kras*^{G12D} and *Trp53*-null (AKP) mutations adapted to the *in vivo* native colonic environment. Comprehensive transcriptomic and chromatin analyses revealed that the endoderm-specifying transcription factor SOX17 became strongly upregulated *in vivo*. Notably, whereas SOX17 loss did not affect AKP organoid propagation *in vitro*, its loss markedly reduced the ability of AKP tumours to persist *in vivo*. The small fraction of SOX17-null tumours that grew displayed notable interferon-γ (IFNγ)-producing effector-like CD8⁺ T cell infiltrates in contrast to the immune-suppressive microenvironment in wild-type counterparts. Mechanistically, in both endogenous *Apc*-null pre-malignant adenomas and transplanted organoid-derived AKP CRCs, SOX17 suppresses the ability of tumour cells to sense and respond to IFNγ, preventing anti-tumour T cell responses. Finally, SOX17 engages a fetal intestinal programme that drives differentiation away from LGR5⁺ tumour cells to produce immune-evasive LGR5[−] tumour cells with lower expression of major histocompatibility complex class I (MHC-I). We propose that SOX17 is a transcription factor that is engaged during the early steps of colon cancer to orchestrate an immune-evasive programme that permits CRC initiation and progression.

CRCs are characterized by a highly immune-suppressive microenvironment^{1,2} that leads to resistance to immunotherapy³. Identifying the mechanisms that orchestrate such immune-dysfunctional ecosystems is crucial to improving current immunotherapy approaches for this disease. Current knowledge is focused on the immune profiling of full-fledged cancers, in which the immune-suppressive environment has already been established. How such an immune-suppressive environment evolves during the early stages of CRC development remains poorly understood.

The adaptive immune system can recognize and eliminate nascent tumours^{4–6}. How cancers evade initial recognition when they are most vulnerable—that is, before they create an immune-suppressive microenvironment—remains poorly understood. This is largely owing to the challenge of detecting tumours as they arise. Mouse models can overcome this limitation and enable insights into the unknowns of immune-cancer cell interactions at the beginning stages of the tumorigenic process.

Here we leveraged a CRC organoid orthotopic transplantation approach^{7,8} and a genetically engineered autochthonous mouse adenoma model^{9,10} to perform a comprehensive epigenomic and transcriptomic analysis to identify the necessary factors that enable tumour initiation in these cancers. We identified SOX17—a transcription factor that is implicated in endoderm and fetal foregut development^{11–13}—as essential for the growth of adenomas and CRCs. SOX17 is not expressed in healthy adult intestinal epithelium but is re-expressed during early tumorigenesis. Loss of SOX17 prevents tumour growth, but only in immunocompetent mice. SOX17 coordinates a fetal reprogramming that actuates an immune-silent phenotype on these nascent cancers by suppressing their ability to respond to IFNγ, which results in decreased antigen presentation and chemokine production. Furthermore, SOX17 alters tumour heterogeneity by driving the differentiation away from LGR5⁺ tumour cells¹⁴ to produce immune-evasive LGR5[−] tumour cells with lower expression of MHC-I. These adaptations

¹Department of Biology, The David H. Koch Institute for Integrative Cancer Research at MIT, Massachusetts Institute of Technology, Cambridge, MA, USA. ²Cold Spring Harbor Laboratory, Cold Spring Harbor, NY, USA. ³Department of Pathology, Massachusetts General Hospital and Harvard Medical School, Boston, MA, USA. ⁴Innovative Genomics Institute, University of California, Berkeley, Berkeley, CA, USA. ⁵Department of Pathology, Beth Israel Deaconess Hospital and Harvard Medical School, Boston, MA, USA. ⁶Department of Cancer Immunology and Virology, Dana-Farber Cancer Institute, Boston, MA, USA. ⁷Department of Immunology, Harvard Medical School, Boston, MA, USA. ⁸Ludwig Center at Harvard, Boston, MA, USA. ⁹Parker Institute for Cancer Immunotherapy at Dana-Farber Cancer Institute, Boston, MA, USA. ¹⁰New York Stem Cell Foundation–Robertson Investigator, New York, NY, USA. ¹¹Broad Institute of MIT and Harvard, Cambridge, MA, USA. ¹²These authors contributed equally: Peter M. K. Westcott, Saori Goto. ¹³These authors jointly supervised this work: Judith Agudo, Ömer H. Yilmaz. [✉]e-mail: judith_agudo@dfci.harvard.edu; ohyilmaz@gmail.com

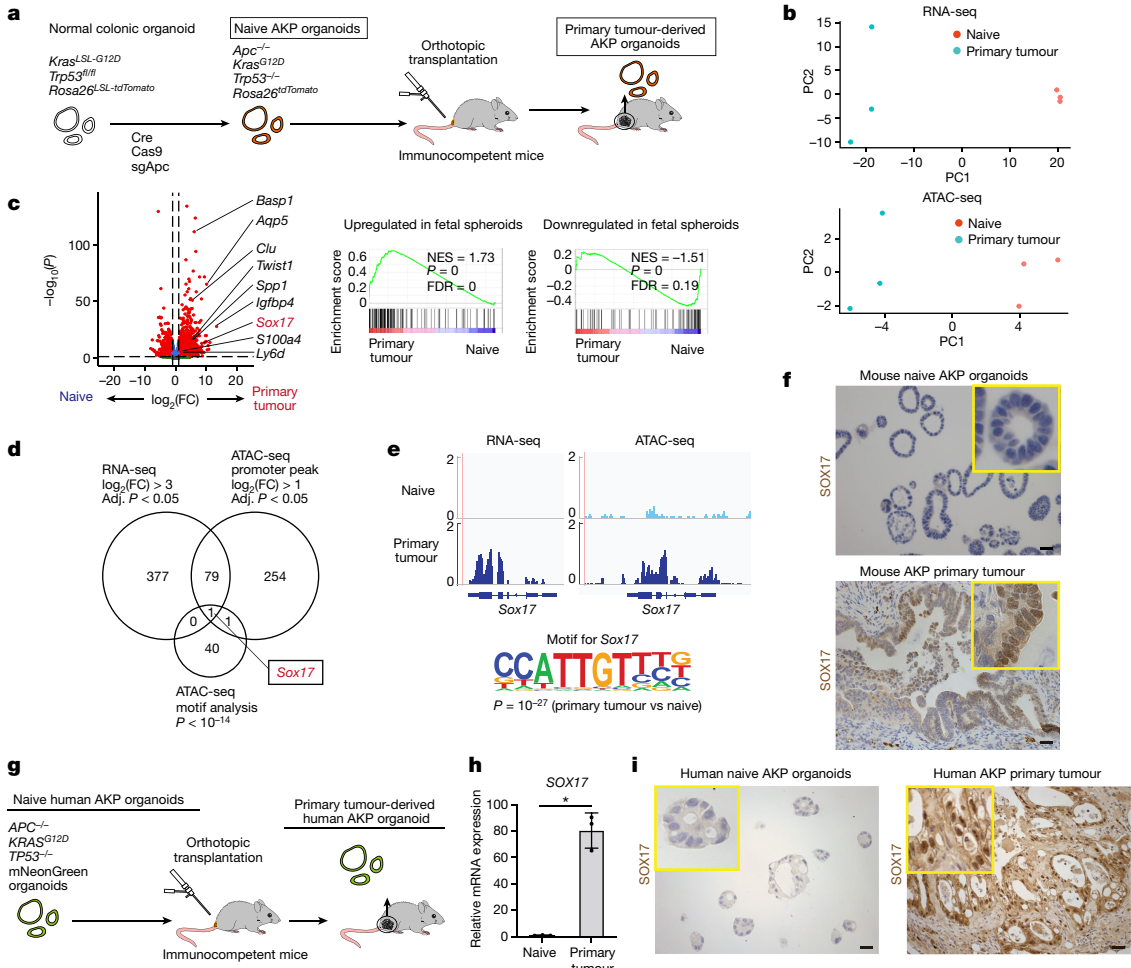


Fig. 1 | Early in vivo epigenetic alterations of AKP CRCs converge on SOX17. **a**, Schematic of generation of mouse naive AKP organoids by CRISPR–Cas9 editing and Cre-mediated recombination, and mouse primary tumour-derived AKP organoids from immunocompetent mice by colonoscopy-based orthotopic transplantation. sgApc, single-guide RNA (sgRNA) targeting *Apc*. **b**, PCA plots of RNA-seq and ATAC-seq in naive and primary tumour-derived AKP organoids. $n = 3$ mice per group. **c**, Volcano plot and GSEA of RNA-seq in naive and primary tumour-derived AKP organoids. FC, fold change; FDR, false discovery rate; NES, normalized enrichment score. **d,e**, Comparison of RNA-seq DGE and ATAC-seq open promoter peak and motif enrichment analyses (**d**). SOX17 is the only transcription factor that is commonly detected in these three analyses (**e**). **f**, IHC of SOX17 in mouse naive AKP organoids and mouse AKP primary tumours. Representative of $n = 10$ mice. Scale bars, 20 μ m. **g**, Schematic of generation of human naive and primary tumour-derived AKP organoids. **h**, RT-qPCR for SOX17 mRNA expression in human naive and primary tumour-derived AKP organoids. $n = 3$ independent recipient mice. Representative of two independent experiments. Unpaired two-tailed *t*-test. **i**, IHC for SOX17 in human naive AKP organoids and human AKP primary tumours in NCG mice. Representative of $n = 6$ mice. Scale bars, 20 μ m. Data are mean \pm s.d. * $P < 0.05$.

enable emergent adenomas and CRCs to evade anti-tumour immune surveillance.

SOX17 is induced in colon tumours

To gain insights into the epigenetic evolution of CRCs, we sought to characterize transcriptomic and epigenetic changes that permit CRC progression *in vivo*. To this end, we leveraged a colonoscopy-based orthotopic transplantation approach⁷⁸ for implanting CRC organoids into the mouse colon. First, we engineered mouse colon cancer organoids harbouring *Apc*, *Kras*^{G12D} and *Trp53* mutations (AKP, a genetic profile seen in 40–45% of patients with CRC¹⁵) with tdTomato fluorescence by CRISPR–Cas9 editing and Cre-mediated recombination from healthy mouse colon organoids (Fig. 1a). We designated these organoids as ‘naive AKP organoids’, indicating that they have oncogenic mutations associated with CRCs *in vitro* but that they have never been tumours *in vivo*. We then orthotopically transplanted these naive AKP organoids into immunocompetent mice by colonoscopy, generated organoids from the resulting primary tumours, and passed them

four to six times as tumour organoids until only tdTomato⁺ tumour cells were present, and all other stromal cells (tdTomato⁻ cells) were excluded from the culture (Fig. 1a). We also passed naive AKP organoids four to six times in parallel with their primary derived counterparts as controls. Given that these naive and primary tumour-derived organoids have the same starting oncogenic drivers, their comparison enabled us to identify stable and heritable epigenetic alterations induced by the *in vivo* environment. Of note, primary tumour-derived AKP organoids presented distinct transcriptomic and chromatin accessibility alterations from naive AKP organoids as illustrated by principal component analysis (PCA) of RNA sequencing (RNA-seq) and assay for transposase-accessible chromatin using sequencing (ATAC-seq) (Fig. 1b). Differential gene expression (DGE) analysis of RNA-seq showed significantly upregulated and downregulated genes (1,074 and 471 genes, respectively, fold change >2 , adjusted *P* value < 0.05) in primary tumour-derived AKP organoids compared with naive AKP organoids (Fig. 1c). We also performed analogous experiments using an orthogonal AKP organoid model, in which APC expression was suppressed by short hairpin RNA (shRNA) targeting

*Apc*¹⁶ (shApc) (Extended Data Fig. 1a). PCA and DGE analysis of RNA-seq data again demonstrated distinct gene expression patterns of primary tumour-derived organoids from those of naive AKP organoids (Extended Data Fig. 1b,c). These results illustrate that the in vivo colon environment induces stable, heritable epigenetic alterations in primary CRC-derived organoids.

We performed motif analysis in open chromatin regions identified by ATAC-seq and found increased chromatin accessibility for transcription factors of the SOX family (SOX2, SOX3, SOX4, SOX6, SOX9, SOX10, SOX15 and SOX17; $P < 10^{-14}$) in primary AKP organoids (Supplementary Table 1), consistent with a study that demonstrated increased chromatin accessibility to SOX family members during human CRC tumour evolution¹⁷. Of note, gene set enrichment analysis (GSEA) of RNA-seq data also revealed an enhancement of a fetal intestinal gene expression signature^{18–20} in primary tumour-derived AKP organoids (Fig. 1c), indicating reactivation of developmental genes in the primary tumour-derived AKP organoids. To identify transcription factors that regulate the transcriptomic and epigenetic alterations in primary tumour-derived AKP organoids, we integrated and compared RNA-seq DGE and ATAC-seq open promoter peak and motif enrichment analyses. SOX17, a transcription factor that is required for endoderm and foregut development^{11–13}, was the sole transcription factor that emerged from these criteria (Fig. 1d,e). Finally, immunohistochemical (IHC) analysis of SOX17 protein in primary in vivo tumours confirmed robust nuclear expression (Fig. 1f). Analogous experiments using our independent shApc AKP organoid model also confirmed significant SOX17 induction in primary tumour-derived organoids. (Extended Data Fig. 1a–c).

We also performed RNA-seq in bulk tumours and in *tdTomato*⁺ tumour cells sorted directly from primary tumours by flow cytometry (Extended Data Fig. 1d) and found that *Sox17* expression and the fetal spheroid-related gene signature were significantly upregulated in in vivo tumours compared with naive AKP organoids (Extended Data Fig. 1e–h). Furthermore, to exclude changes that may arise from organoid cultures and transplantation, we induced autochthonous AKP tumours in *Villin*^{creERT2}, *Apc*^{f/f}, *Kras*^{LSL-G12D}, *Trp53*^{f/f}; *Rosa26*^{LSL-tdTomato} (AKPVT) mice with colonoscopy-guided injection of 4-hydroxy tamoxifen into the colonic mucosa⁷ (Extended Data Fig. 2a). RNA-seq of these endogenous AKPVT tumours confirmed significant expression of *Sox17* and the fetal spheroid gene signature compared with normal colonic epithelium (Extended Data Fig. 2b–d).

Next, we sought to ascertain the role of immune cells in the induction of SOX17 in vivo. We transplanted AKP organoids into immunodeficient *Rag2*^{−/−} mice (that is, mice that lack B and T cells; Extended Data Fig. 2e). PCA and DGE analyses of RNA-seq data from AKP organoids derived from *Rag2*^{−/−} mice also showed notable SOX17 upregulation compared with naive AKP organoids (Extended Data Fig. 2e–g). To confirm that SOX17 expression is also induced in human AKP organoids in vivo, we engineered naive AKP organoids from human colonic organoids using CRISPR–Cas9 genome editing (Extended Data Fig. 3a–f), orthotopically transplanted these human AKP organoids into immunodeficient mouse (NCG mouse) colons, and established AKP organoid lines from the primary tumours (Fig. 1g). Similar to our studies in AKP mice, primary tumour-derived human AKP organoids showed significantly higher expression of SOX17 compared with their naive counterparts, as detected by quantitative PCR with reverse transcription (RT–qPCR) (Fig. 1h), IHC (Fig. 1i) and immunoblots (Extended Data Fig. 3g). Together, our data implicate SOX17 as a transcription factor that is induced in early AKP CRCs in the in vivo colonic environment in both mouse and human colon cells.

SOX17 prevents immune clearance

To ascertain the role of SOX17 in colonic tumorigenesis, we ablated SOX17 expression in in vivo tumour-derived AKP organoids with CRISPR–Cas9 editing (Fig. 2a and Supplementary Fig. 2a–c) and

confirmed its loss by immunoblot (Fig. 2b) and IHC (Extended Data Fig. 4a). SOX17 loss in in vivo tumour-derived AKP organoids did not affect their growth and proliferation in culture (Fig. 2c and Extended Data Fig. 4b–d). However, when these SOX17-null AKP organoids were transplanted into the colons of immunocompetent mice, only around 6% of recipients developed tumours (Fig. 2d–f), which were significantly reduced in size (Fig. 2g and Extended Data Fig. 4e), compared with around 80% of recipients when transplanted with control organoids.

Consistent with prior reports^{3,16,21}, control AKP tumours were poorly infiltrated and ‘immune cold’ (Fig. 2h, i), whereas the few surviving SOX17-null tumours displayed robust intra-tumoral infiltration of immune cells, including many CD4⁺ and CD8⁺ T cells (Fig. 2h,i). These results indicate that SOX17 expression in vivo may be crucial in suppressing anti-tumour immune responses. To test this notion, we transplanted SOX17-null AKP organoids into immunodeficient NCG mice or *Rag2*^{−/−} mice (Fig. 2j). We observed that all recipient mice developed tumours with no significant difference in tumour size (Fig. 2k,l) or in the number of Ki67⁺ cells (Extended Data Fig. 4f–i) compared to control tumours, demonstrating that SOX17 promotes tumour establishment and growth through immune cells. To determine whether SOX17 suppression also hinders the growth of established AKP tumours, we suppressed SOX17 expression using a shRNA doxycycline-inducible system (Extended Data Fig. 5a–d). *Sox17* knockdown hindered tumour growth and significantly increased infiltration of CD4⁺ and CD8⁺ T cells in established tumours (Extended Data Fig. 5e–h), indicating that SOX17 permits tumour progression by preventing immune clearance.

SOX17 suppresses IFN γ signalling

To decipher how SOX17 in tumour cells controls the evolution of the tumour-associated immune milieu, we performed single-cell RNA-seq (scRNA-seq) on flow cytometry-sorted CD45⁺ cells from control and SOX17-null tumours collected from immunocompetent recipients at 1, 2 and 4 weeks post-transplantation (Extended Data Fig. 6a–c). At week 1, nascent tumours were infiltrated mostly by myeloid cells (macrophages and neutrophils) in control and SOX17-null tumours (Extended Data Fig. 7a,b). At week 2, along with these myeloid populations, control and SOX17-null tumours showed infiltration of CD4⁺ and CD8⁺ T cells (Extended Data Fig. 7a,b). At week 4, however, immune populations diverged between control and SOX17-null tumours: whereas control tumours retained suppressive neutrophils and infiltrating CD8⁺ T cells displayed exhaustion signatures, SOX17-null tumours exhibited an expansion of CD8⁺ T cells with high expression of *Ifng* (Extended Data Figs. 6c and 7a,b). We further re-clustered T cells to gain insights into how they changed (Fig. 3a,b). In control tumours, terminally exhausted CD8⁺ T cells (expressing markers such as *Tox*, *Tigit*, *Lag3*, *Havcr2*, *Pdcd1*, *Cd38*, *Gzma* and *Gzmb*^{22–24}, Fig. 3c) constituted the major population of CD8⁺ T cells at week 4 (29%) (Fig. 3a–c), consistent with previous reports¹⁶. However, in SOX17-null tumours at the same timepoint, the numbers of terminally exhausted CD8⁺ T cells were markedly decreased (2.3%) (Fig. 3a–c), and effector-like CD8⁺ T cells (expressing markers such as *Ifng*, *Cxcr6* and *Cd28*; Fig. 3c), which have potent anti-tumour killing capacity²⁵, became the largest population (70.7%) (Fig. 3a,b). Conversely, this cytotoxic population was only sparsely detected in control tumours (0.6%) (Fig. 3a,b), consistent with the immune-suppressive environment of CRCs^{1,2,16}.

Re-clustering of CD4⁺ T cells revealed three subclusters: regulatory T (T_{reg}) cells, T helper 1 (T_{H1}) effector CD4⁺ T cells (expressing markers such as *Tbx21*, *Cd40lg* and *Cd28*), and CD4⁺ T cells with markers of exhaustion (*Pdcd1*, *Tox* and *Lag3*) (Extended Data Fig. 7c–e). In the control tumours, T_{reg} cells (57.6%) were the predominant CD4⁺ T cell populations at week 4; conversely, in the SOX17-null tumours, effector T_{H1} cells, which have a critical role in the activation and cytotoxic function of CD8⁺ T cells, became the dominant (85.2%) CD4⁺ T cell type

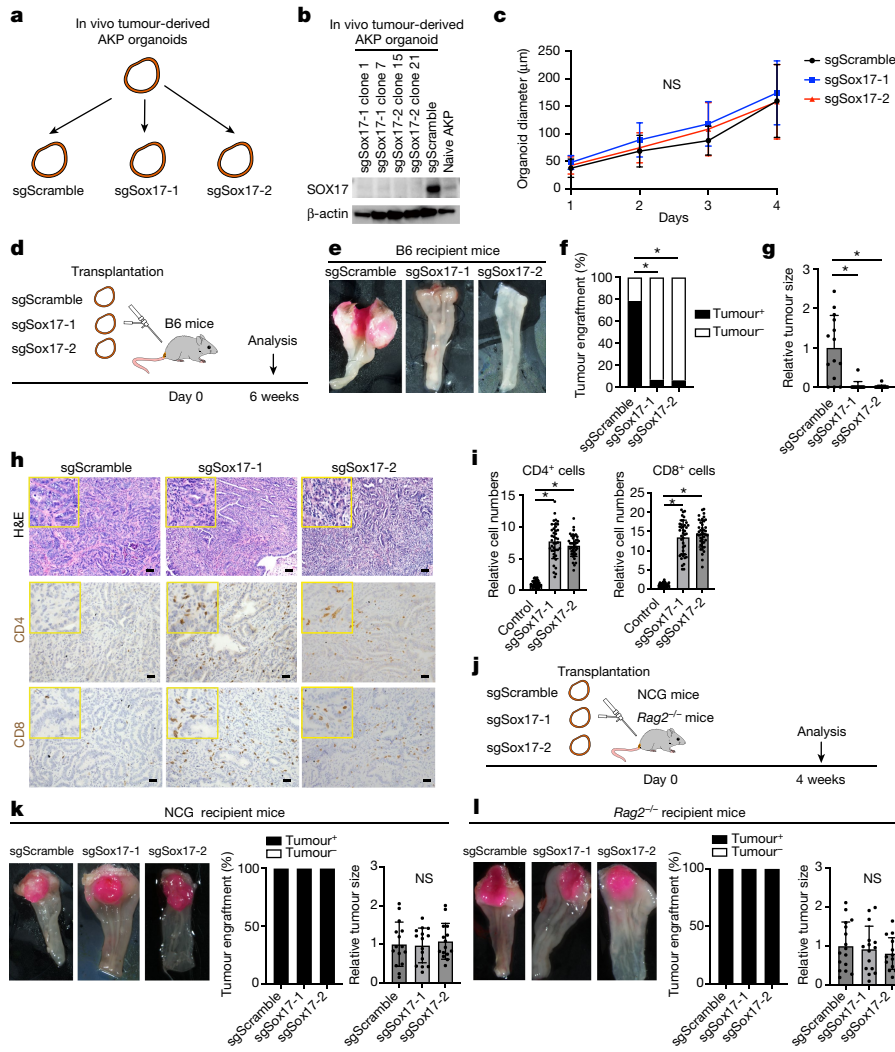


Fig. 2 | SOX17 loss leads to immune-mediated rejection of colon tumours.

a, Generation of SOX17-knockout (SOX17-KO) in vivo tumour-derived AKP organoids using two different sgRNAs targeting *Sox17* (sgSox17-1 and sgSox17-2) and a control sgRNA (sgScramble). **b**, Immunoblots for SOX17 in naive AKP organoids, using in vivo tumour-derived AKP control (sgScramble) organoids or four different lines of SOX17-KO organoids (two sgRNAs, sgSox17-1 and sgSox17-2). **c**, Growth curve of sgScramble, sgSox17-1 and sgSox17-2 AKP organoids. $n = 30$ organoids from 10 wells per group. **d–g**, Schematic (**d**), representative images (**e**), tumour engraftment rate (**f**) and tumour size (**g**) following orthotopic transplantation of sgScramble, sgSox17-1 and sgSox17-2 AKP organoids into the colons of immunocompetent mice. $n = 14\text{--}16$ mice per group. **h**, Haematoxylin

and eosin (H&E) staining and IHC for CD4 and CD8 in sgScramble, sgSox17-1 and sgSox17-2 AKP tumours. Scale bars, 20 μm . **i**, Quantification of CD4⁺ and CD8⁺ cells in sgScramble, sgSox17-1 and sgSox17-2 AKP tumours. $n = 40$ fields from 5 mice per group, pooled from 4 independent experiments. **j**, Schematic of orthotopic transplantation of sgScramble, sgSox17-1 and sgSox17-2 AKP organoids into the colons of immunodeficient mice. **k,l**, Representative images, tumour engraftment rate and tumour size of orthotopic transplantation of sgScramble, sgSox17-1, and sgSox17-2 AKP organoids into the colons of NCG mice (**k**) and *Rag2*^{-/-} mice (**l**). $n = 15\text{--}16$ mice per group. Pooled from three independent experiments. One-way analysis of variance (ANOVA) (**c,g,i,k,l**); chi-square test (**f**). Data are mean \pm s.d. NS, not significant.

(Extended Data Fig. 7c–e). Thus, our analysis indicates that in control tumours, an incipient adaptive immune response is dampened by suppressive myeloid cells and exhaustion of T cells; conversely, the lack of SOX17 in tumour cells supports this initial immune response leading to a significant accumulation of effector CD8⁺ T cells and T_H1 CD4⁺ T cells.

To further validate these findings, we quantified CD8⁺ and CD4⁺ T cells on tissue sections by IHC at weeks 1, 2 and 4 (Fig. 3d,e and Extended Data Fig. 8a–c). Control tumours showed an increase in T cell infiltration in week 2 compared with week 1, as demonstrated in the scRNA-seq analysis and in agreement with the timing required for an adaptive immune response to occur. These infiltrates were then reduced in control tumours at week 4, as the tumours grew and acquired suppressive microenvironments. By contrast, SOX17-null tumours exhibited further increased infiltrating T cells at week 4, as the anti-tumour immune response is amplified. Flow cytometry analysis

confirmed that CD8⁺ T cells in SOX17-null tumours had significantly higher capacity to produce IFN γ and TNF (features of activated CD8⁺ effector T cells) compared with control tumours (Fig. 3f,g), and consistent with the scRNA-seq results (Fig. 3a–c). Among IFN γ -producing cells (T cells and natural killer cells), effector-like CD8⁺ T cells were the largest in SOX17-null tumours (Extended Data Fig. 8d).

These results prompted us to investigate the function of CD8⁺ and CD4⁺ T cells in mediating the effects of SOX17 in tumours. CD8⁺ T cell depletion allowed all SOX17-null tumours to grow (Fig. 3h–j), indicating that SOX17-null tumours are eliminated by CD8⁺ T cells in immunocompetent mice. CD4⁺ T cell depletion, albeit to a lesser extent, also rescued engraftment of SOX17-null tumours (Extended Data Fig. 8e–g). The size of tumours from CD4⁺ T cell-depleted mice was significantly smaller compared with mice lacking CD8⁺ T cells (Extended Data Fig. 8h). These data indicate that T_H1 cells in SOX17-null tumours probably support the

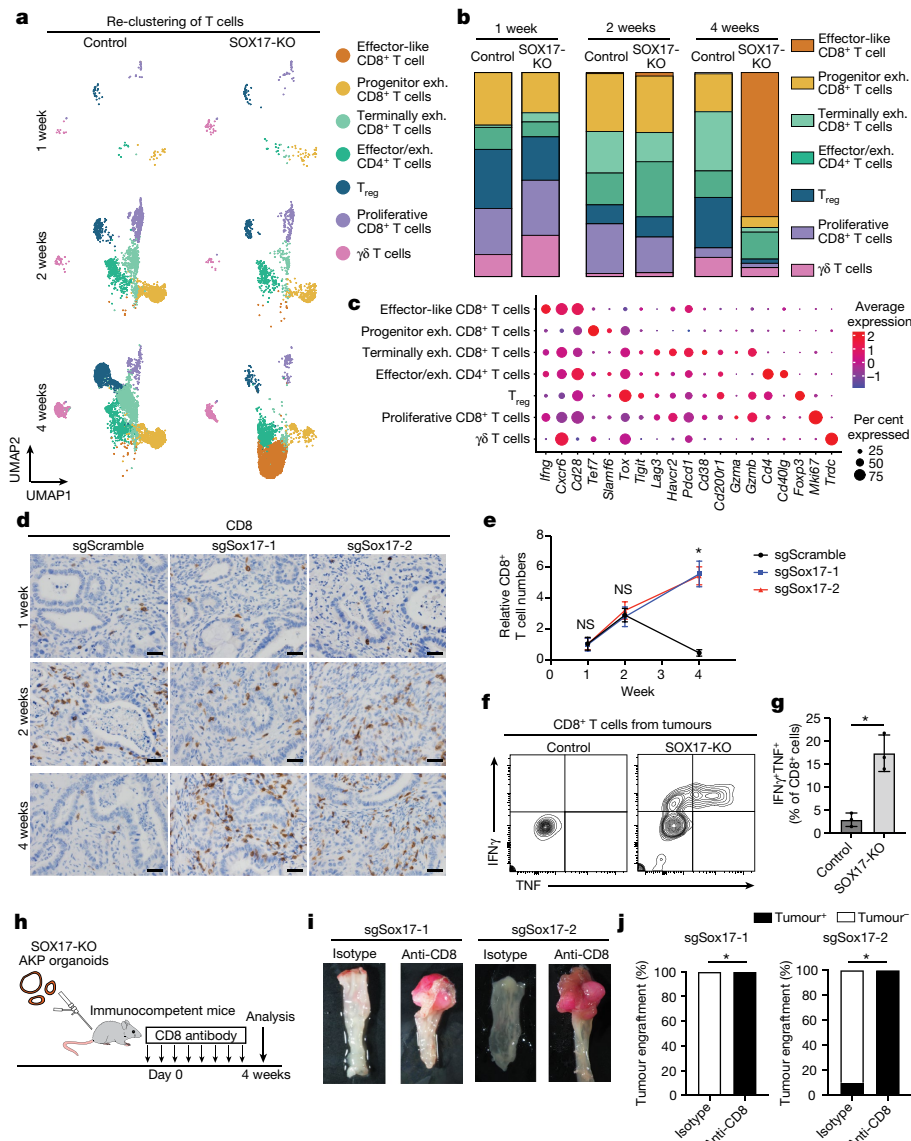


Fig. 3 | SOX17 suppresses CD8⁺ T cell-mediated tumour elimination via IFN γ signalling. **a–c.** Analysis of re-clustered T cells from scRNA-seq of CD45⁺ cells in control and SOX17-KO AKP tumours at 1, 2 and 4 weeks post-transplantation (see also Extended Data Fig. 7). Uniform manifold approximation and projection (UMAP) of the re-clustered T cells (**a**), bar graphs showing the proportion of cells in each subcluster (**b**) and dot plots of gene expression in each subcluster (**c**). 1-week control, $n = 93$ cells; 2-week control, $n = 2,216$ cells; 4-week control, $n = 4,097$ cells; 1-week SOX17-KO, $n = 178$ cells; 2-week SOX17-KO, $n = 810$ cells; 4-week SOX17-KO, $n = 4,724$ cells. Pooled from 5 mice in each group. Exh., exhausted. **d,e.** Representative images (**d**) and quantification (**e**) of IHC of CD8

in sgScramble, sgSox17-1 and sgSox17-2 AKP tumours at 1, 2 and 4 weeks post-transplantation. $n = 20$ fields from 5 mice per group. One-way ANOVA. Scale bars, 20 μ m. **f,g.** Flow cytometry of IFN γ and TNF in CD8⁺ T cells (**f**; see also Supplementary Fig. 3 and Methods for details) and quantification of IFN γ TNF⁺ cells per CD8⁺ cells (**g**) in control and SOX17-KO (sgSox17-1) tumours. $n = 3$ mice per group. Unpaired two-tailed *t*-test. **h–j.** Schematic (**h**), representative images (**i**) and tumour engraftment rate (**j**) of orthotopic transplantation of SOX17-KO (sgSox17-1 and sgSox17-2 lines) AKP organoids into the colons of anti-CD8-treated mice. $n = 9–10$ mice per group, pooled from 2 independent experiments. Fisher's exact test. Data are mean \pm s.d.

anti-tumour CD8⁺ T cell-mediated response. In support of this notion, the numbers of CD8⁺ T cells in tumours of CD4⁺ T cell-depleted mice were significantly decreased compared with controls (Extended Data Fig. 8i,j). Collectively, these data illustrate that effector-like CD8⁺ T cells actuate the rejection of SOX17-null tumours, and that CD4⁺ effector T_H1 cells have an essential role in sustaining and enhancing CD8⁺ T cell responses.

To further delineate the role of CD8⁺ T cell-mediated tumour cell killing of SOX17-null tumours, we deleted *H2k1* or *B2m*, components of the MHC-I, in SOX17-null AKP organoids (Extended Data Fig. 9a,b) and transplanted them into immunocompetent mice (Extended Data Fig. 9c). Deficiency of either *H2k1* or *B2m* rescued the ability of SOX17-null tumours to engraft (Extended Data Fig. 9d,e), again supporting the

notion that SOX17-null tumours are eliminated by CD8⁺ T cell-mediated tumour cell killing.

Next, we sought to address whether SOX17 was able to directly induce intrinsic resistance of tumour cells to effector CD8⁺ T cell elimination, independent of repressing T cell infiltration, by heterotypically co-culturing colon cancer organoid and CD8⁺ T cell co-cultures. We constitutively overexpressed SOX17 (SOX17-OE) in colon cancer organoids expressing the ovalbumin immune-dominant antigen SIINFKEL¹⁶ and co-cultured them with pre-activated ovalbumin-specific OT-1 CD8⁺ T cells (Extended Data Fig. 9f). Whereas control organoids were mostly eliminated by day 6, SOX17-OE organoids were more resistant to direct OT-1 T cell-mediated killing (Extended Data Fig. 9g,h). Correspondingly, fewer infiltrating CD8⁺ OT-1 cells were observed in the Matrigel matrix

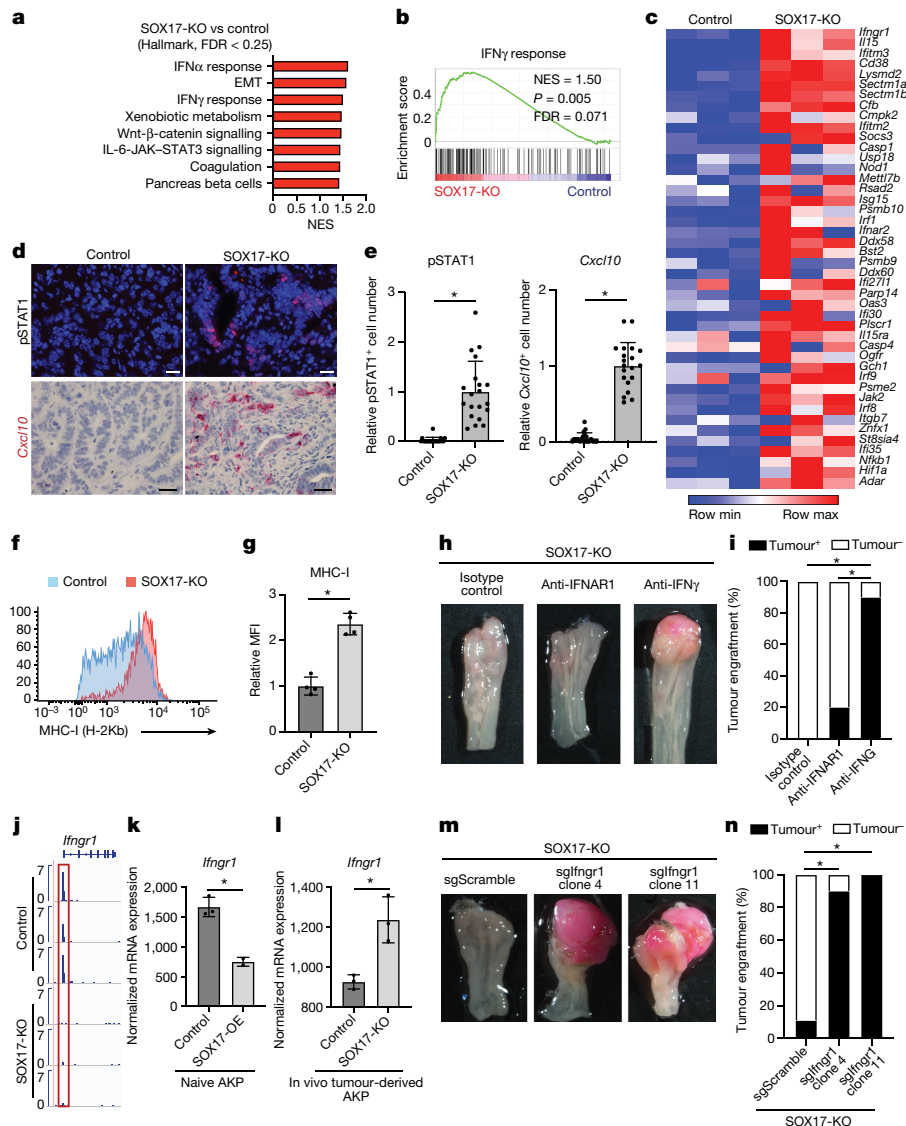


Fig. 4 | SOX17 suppresses IFN γ -mediated MHC-I expression to evade CD8 $^{+}$ T cell-mediated tumour cell killing. **a–c**, RNA-seq in control and SOX17-KO AKP organoids. GSEA using Hallmark gene sets in the Molecular Signatures Database (**a**; FDR < 0.25) and enrichment scores for genes in the IFN γ -response gene set (**b**). **c**, Heat map of IFN γ signalling pathway genes (*Ifngr1* plus top-ranked genes of the IFN γ -response gene set in rank order). *n* = 3 organoid clones per group. Control, sgScramble clones 26, 27 and 28; SOX17-KO, sgSox17-1 clones 1 and 7, sgSox17-2 clone 15 (Supplementary Fig. 2). **d,e**, Representative images (**d**) and quantification (**e**) of immunofluorescence for pSTAT1 and *In situ* hybridization for *Cxcl10* in control and SOX17-KO (sgSox17-1) tumours at 6 weeks post-transplantation. *n* = 20 fields from 5 mice. Scale bars, 20 μ m. **f,g**, Flow cytometry (**f**) and quantification (**g**) of MHC-I (also known as H-2Kb) expression in control and SOX17-KO (sgSox17-1) tumours at 2 weeks post-transplantation. *n* = 4 mice per group. **h,i**, Representative images (**h**) and tumour engraftment rate (**i**) of orthotopically transplanted SOX17-KO (sgSox17-1) AKP tumours in mice treated with isotype control, anti-IFNAR1 or anti-IFN γ . **j**, CUT&RUN for SOX17 showed SOX17 binding to the *Ifngr1* promoter. *n* = 3 different organoid lines per group. **k,l**, *Ifngr1* mRNA expression in RNA-seq analysis of control versus doxycycline-inducible and constitutive SOX17-OE naive AKP organoids (**k**) and control versus SOX17-KO *in vivo* tumour-derived AKP organoids (**l**). *n* = 2–3 per group. **m,n**, Representative images (**m**) and tumour engraftment rate (**n**) of orthotopic transplantation of SOX17-KO (sgSox17-1), sgScramble, SOX17-KO (sgSox17-1) and IFN γ knockout (sgIfngr1 clones 4 and 11) AKP organoids into the colons of immunocompetent mice. *n* = 9–10 mice per group. Unpaired two-tailed *t*-tests (**e,g,k,l**); chi-square tests (**i,n**). Data are mean \pm s.d.

weeks post-transplantation. *n* = 4 mice per group. **h,i**, Representative images (**h**) and tumour engraftment rate (**i**) of orthotopically transplanted SOX17-KO (sgSox17-1) AKP tumours in mice treated with isotype control, anti-IFNAR1 or anti-IFN γ . **j**, CUT&RUN for SOX17 showed SOX17 binding to the *Ifngr1* promoter. *n* = 3 different organoid lines per group. **k,l**, *Ifngr1* mRNA expression in RNA-seq analysis of control versus doxycycline-inducible and constitutive SOX17-OE naive AKP organoids (**k**) and control versus SOX17-KO *in vivo* tumour-derived AKP organoids (**l**). *n* = 2–3 per group. **m,n**, Representative images (**m**) and tumour engraftment rate (**n**) of orthotopic transplantation of SOX17-KO (sgSox17-1), sgScramble, SOX17-KO (sgSox17-1) and IFN γ knockout (sgIfngr1 clones 4 and 11) AKP organoids into the colons of immunocompetent mice. *n* = 9–10 mice per group. Unpaired two-tailed *t*-tests (**e,g,k,l**); chi-square tests (**i,n**). Data are mean \pm s.d.

of SIIINFEKL-expressing SOX17-OE versus control organoids (Extended Data Fig. 9i), indicating that tumour cell SOX17 expression augments colon cancer cell resistance to CD8 $^{+}$ T cell-mediated killing.

To decipher the mechanism by which failure to induce SOX17 in cancer cells makes them more immunogenic and susceptible to CD8 $^{+}$ T cell recognition and killing, we performed RNA-seq on cultured control and SOX17-null mouse AKP organoids (Supplementary Fig. 2c). GSEA revealed that a IFN γ response gene set was one of the top pathways upregulated in SOX17-null AKP organoids *in vitro* (Fig. 4a,b). IFN γ signalling pathway genes that were enriched in SOX17-null organoids included one of the two subunits of the receptor for IFN γ (*Ifngr1*),

antigen processing and presentation genes (*Psmib9* and *Psmib10*), interferon-induced transmembrane proteins (*Ifitm2* and *Ifitm3*), IL-15 related-genes (*Il15* and *Il15ra*), the innate immune sensor RIG-I (*Ddx58*) and other inflammatory signalling molecules (*Jak2* and *Nfkb1*) (Fig. 4c). We tested whether the IFN γ signalling pathway was also upregulated in SOX17-null tumours *in vivo* by performing immunofluorescence for phosphorylated STAT1 (pSTAT1), which is induced upon IFN γ receptor signalling activation²⁶. pSTAT1 was robustly detected in SOX17-null tumours compared with controls (Fig. 4d,e), indicating an enhanced response to IFN γ in SOX17-null tumour cells. Augmented IFN γ signalling in cancer cells leads to recruitment of activated CD8 $^{+}$ T cells^{27,28}

Article

by increasing chemotaxis and antigen presentation. We assessed the levels of MHC-I in SOX17-null tumours and found that they have significantly higher expression of MHC-I compared with control tumours (Fig. 4f,g). Additionally, *Cxcl10*, an IFN γ -induced chemokine that attracts CD8 $^{+}$ T cells²⁹, was enriched in SOX17-null tumours (Fig. 4d,e). Thus, SOX17-null colon cancer cells are poised to respond strongly to IFN γ , which increases their immunogenicity and recruitment by augmenting expression of MHC-I and CXCL10, respectively, facilitating their rejection by CD8 $^{+}$ T cells. GSEA predicted that the IFN α -response gene set is also upregulated in SOX17-null AKP organoids (Fig. 4a), but the expression of both subunits of its receptor (*Ifnar1* and *Ifnar2*) was not affected by loss of SOX17 (Extended Data Fig. 9j–l). To decipher which IFN signalling pathway (type I or II) was critical for the rejection of SOX17-null tumours, we treated mice with either a neutralizing antibody for IFN γ or a blocking antibody for IFNAR1, and assessed SOX17-null tumour engraftment. Whereas IFNAR1 blockade did not rescue SOX17-null tumour engraftment, IFN γ neutralization significantly boosted SOX17-null tumour engraftment with 90% of tumours growing in immunocompetent mice (Fig. 4h,i). Thus, SOX17 induction during in vivo tumorigenesis represses the ability of tumour cells to sense and respond to IFN γ , protecting them from immune recognition and sustaining tumour progression.

To investigate the mechanism by which SOX17 dampens IFN γ signalling in colon cancer cells, we performed cleavage under targets and release using nuclease (CUT&RUN) for SOX17 and found that SOX17 directly binds to the *Ifngr1* promoter (Fig. 4j). To recapitulate the strong induction of SOX17 that occurs in vivo in organoid cultures, we introduced doxycycline-inducible and constitutive SOX17-OE constructs to naive AKP organoids (Extended Data Fig. 10a–d) and found that SOX17-OE notably downregulated *Ifngr1* expression (Fig. 4k and Extended Data Fig. 10e), whereas SOX17 loss significantly upregulated its expression (Fig. 4l). Given that (1) SOX17 directly suppressed *Ifngr1* expression, (2) SOX17-null tumours showed a heightened IFN γ response, and (3) IFN γ neutralization rescued the engraftment of SOX17-null tumours (Fig. 4h,i), we postulated that the rejection of SOX17-null tumours in the immunocompetent recipient mice is mediated by hyperactivation of this pathway. To test this possibility, we deleted IFNGR1 in SOX17-null AKP organoids and orthotopically transplanted them into immunocompetent mice. IFNGR1 protein loss was confirmed by flow cytometry (Extended Data Fig. 10f–h), and its functional loss was confirmed by the inability of AKP cells to upregulate MHC-I after IFN γ administration (Extended Data Fig. 10i,j). Of note, IFNGR1 loss restored the ability of SOX17-null tumours to engraft (Fig. 4m,n), demonstrating that high sensitivity to IFN γ in the SOX17-null tumours contributes to their rejection in immunocompetent recipient mice. We also disrupted CXCL10, an IFN γ -induced chemokine that attracts CD8 $^{+}$ T cells²⁹, in the SOX17-null organoids and transplanted them in immunocompetent mice. CXCL10 loss partially rescued SOX17-null tumour engraftment (Extended Data Fig. 11a–c), indicating that tumour-derived CXCL10 in SOX17-null tumours contributes to their rejection through the recruitment of immune cells. These results indicate that SOX17 in vivo induction represses the expression of key genes in the IFN γ signalling cascade in cancer cells, preventing a feedforward loop of recruiting activated IFN γ -producing effector-like CD8 $^{+}$ T cells. This effectively prevents the formation of anti-tumour T cell responses, protecting these colon cancers from immune clearance.

SOX17 allows immune escape of adenomas

APC loss in LGR5 $^{+}$ intestinal stem cells initiates the cascade of events that leads to the formation of pre-malignant adenomas⁹. Over time, these adenomas progress to invasive colonic adenocarcinomas by acquiring additional mutations in oncogenes such as *KRAS* and *TP53* (ref. 30). Next, we assessed which step of the adenoma–carcinoma sequence SOX17 expression was induced in vivo. To recapitulate the initial steps of adenoma formation, we first induced APC loss by colonoscopy-guided

4-OH-tamoxifen injection into the colonic mucosa of *Villin*^{creERT2}; *Apc*^{f/f} mice⁷ to generate *Apc*-null adenomas. Whereas SOX17 was not detected in normal colonic epithelial cells, mouse adenomas were robustly and diffusely SOX17-positive (Extended Data Fig. 11d). Given that SOX17 expression in AKP organoids was induced when transplanted in vivo (Fig. 1a–f), we tested whether this was also the case for *Apc*-null organoids by generating naïve and primary tumour-derived *Apc*-null organoids (Extended Data Fig. 11e). Similar to AKP organoids, primary tumour-derived *Apc*-null organoids exhibited significantly higher expression of *Sox17* compared with their naïve counterparts (Extended Data Fig. 11f), highlighting that the colon environment induces SOX17 expression in vivo at the pre-malignant phase of CRCs.

To assess the necessity for SOX17 at this early stage of tumorigenesis, we generated *Lgr5*^{creERT2}; *Apc*^{f/f}; *Sox17*^{v/v} mice to concomitantly delete APC and SOX17 in LGR5 $^{+}$ intestinal stem cells in vivo. Whereas *Lgr5*^{creERT2}; *Apc*^{f/f} mice effectively developed adenomas, tumour burden was substantially reduced upon loss of SOX17 in *Lgr5*^{creERT2}; *Apc*^{f/f}; *Sox17*^{v/v} mice, as assessed by adenomatous morphology and nuclear accumulation of beta-catenin (Fig. 5a,b and Extended Data Fig. 11g), revealing an essential role for SOX17 in adenoma formation. As in our AKP transplant model, SOX17 expression anti-correlated with the presence of CD4 $^{+}$ and CD8 $^{+}$ T cells (Fig. 5c,d). These results demonstrate that SOX17, even at the earliest stages of adenomatous dysplasia (that is, adenoma formation by APC loss), averts the immune recognition of incipient tumours.

To test the role of CD8 $^{+}$ T cells in this process, we depleted CD8 $^{+}$ T cells by administration of anti-CD8a antibody and then induced concomitant loss of APC and SOX17 by tamoxifen injection (Fig. 5e). Notably, depletion of CD8 $^{+}$ T cells rescued tumour formation in *Lgr5*^{creERT2}; *Apc*^{f/f}; *Sox17*^{v/v} mice (Fig. 5f,g), indicating that SOX17 expression in nascent *Apc*-null tumours protects them against CD8 $^{+}$ T cell-mediated elimination. This autochthonous *Apc* tumour model complements analogous results observed in the orthotopic transplantation model using the more aggressive AKP genotype (Fig. 3h–j) and demonstrates that SOX17 mediates an immune-evasion programme in both early AKP CRCs and its antecedent pre-malignant adenoma.

Human adenomas and CRCs express SOX17

We next sought to assess whether SOX17 is similarly induced in human adenomas and CRCs as it is in mice. We performed IHC for SOX17 and CD8 in patient samples of adenomas and CRCs at pathologic tumour stages 1 to 4 (pT1 to pT4). First, we classified all samples into SOX17^{hi} ($\geq 70\%$), SOX17^{mid} ($< 70\%, \geq 30\%$), SOX17^{low} ($< 30\%, > 0\%$) and SOX17⁰ (0%) based on the percentage of cells with positive SOX17 nuclear staining. In patient adenomas, all samples ($n = 19$) were SOX17^{hi/mid} and poorly infiltrated with CD8 $^{+}$ T cells (Extended Data Fig. 12a,b) in agreement with our mouse data. All pT1 early-stage CRC samples in patient CRCs were SOX17^{hi/mid} and poorly infiltrated with CD8 $^{+}$ T cells. In more advanced stages (pT2–pT4) 70–80% of tumours were SOX17^{hi/mid}, and the rest were SOX17^{low/neg} (Extended Data Fig. 12c,d), indicating that a fraction of more advanced CRCs downregulate SOX17. At these later stages, most cases were poorly infiltrated with CD8 $^{+}$ T cells, but there were some cases (20–30%) with high CD8 $^{+}$ T cell infiltrates; notably, these CD8 $^{+}$ T cell high tumours were significantly enriched in the cohort of SOX17^{low} cases (Extended Data Fig. 12c–e). Overall, these data support the notion that SOX17 expression is uniformly strong in pre-malignant adenomas and early CRCs, and its expression anti-correlates with CD8 $^{+}$ T cells, thereby contributing to the immune escape of early dysplastic and cancerous colorectal human cells.

SOX17 induces immune-silent LGR5 $^{-}$ cells

Histological examination of *Lgr5*^{creERT2}; *Apc*-null adenomas revealed that SOX17 was expressed in the upper compartment of the tumours and

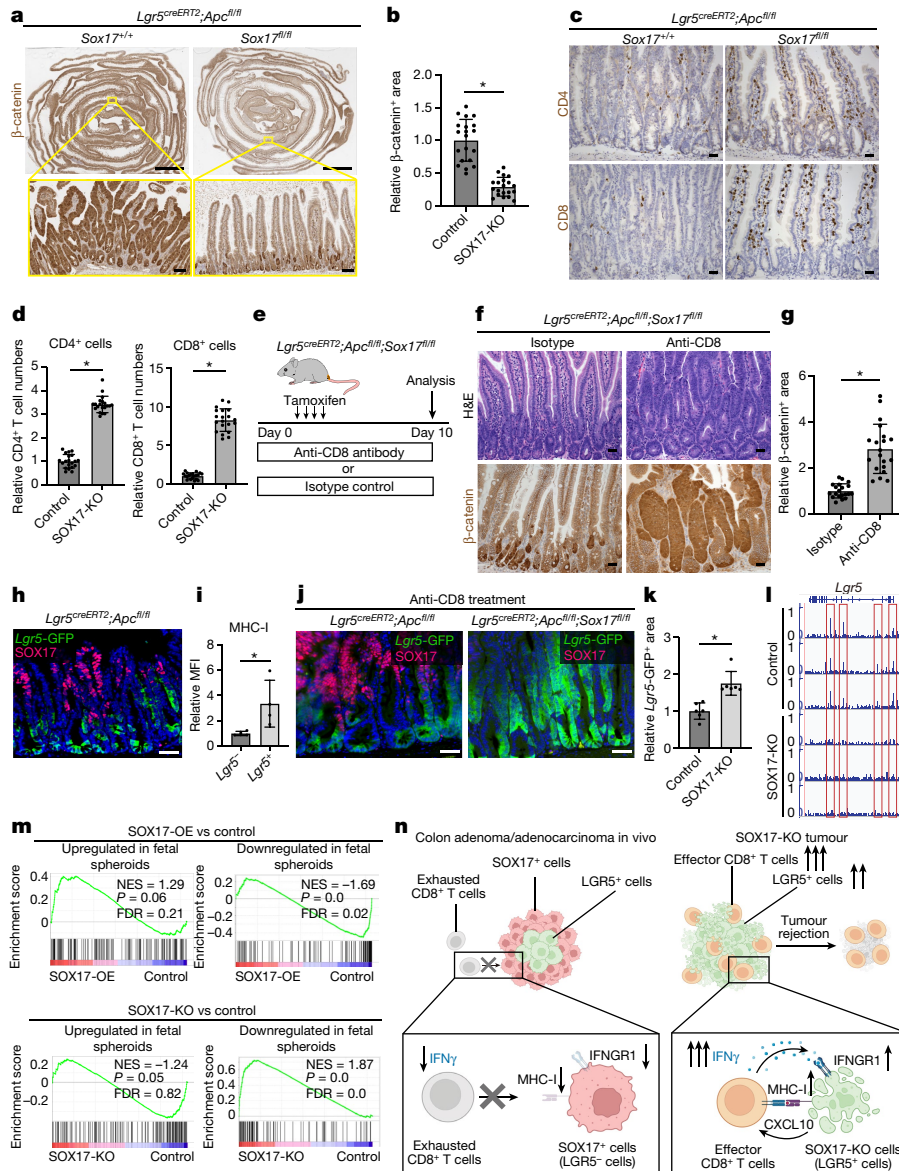


Fig. 5 | SOX17 produces LGR5⁻ cells to evade anti-tumour immunity.

a–d, IHC of β -catenin (**a**) and quantification of nuclear β -catenin-positive tumour cell areas (**b**) in $Lgr5^{creERT2};Apc^{fl/fl}$ and $Lgr5^{creERT2};Apc^{fl/fl};Sox17^{fl/fl}$ mouse intestines. IHC for CD4 and CD8 (**c**) and quantification of CD4⁺ and CD8⁺ cell numbers (**d**). $n = 20$ fields from 5 mice per group. Experiments were repeated three times. **e–g**, Schematic of anti-CD8 treatment of $Lgr5^{creERT2};Apc^{fl/fl};Sox17^{fl/fl}$ mice with tamoxifen injections (**e**), H&E staining and IHC for β -catenin in anti-CD8-treated or isotype antibody-treated $Lgr5^{creERT2};Apc^{fl/fl};Sox17^{fl/fl}$ mouse intestines (**f**) and quantification of β -catenin nuclear accumulation-positive tumour cell areas (**g**). $n = 20$ fields from 5 mice per group. Experiments were repeated three times. **h**, Immunofluorescence of $Lgr5$ -GFP and SOX17 in $Lgr5^{creERT2};Apc^{fl/fl}$ adenoma. Representative of $n = 6$ mice. **i**, Quantification of MHC-I

expression in $Lgr5$ -GFP⁻ and $Lgr5$ -GFP⁺ cells from $Lgr5^{creERT2};Apc^{-/-}$ adenoma. $n = 4$ mice. MFI, mean fluorescence intensity. **j, k**, Immunofluorescence (**j**) of $Lgr5$ -GFP and SOX17 in anti-CD8-treated $Lgr5^{creERT2};Apc^{fl/fl}$ and $Lgr5^{creERT2};Apc^{fl/fl};Sox17^{fl/fl}$ mouse intestinal tumours and quantification of $Lgr5$ -GFP⁺ area (**k**). $n = 6$ fields from 5 mice per group. **l**, CUT&RUN for SOX17 shows SOX17 binding to the $Lgr5$ promoter and introns. $n = 3$ per group. **m**, GSEA using fetal intestinal marker genes in RNA-seq data of control and SOX17-OE naive AKP organoids and control and SOX17-KO in vivo tumour-derived AKP organoids. **n**, Schematic showing the role of SOX17 in immune evasion of colon adenoma/adenocarcinoma. Unpaired two-tailed t -tests (**b, d, g, i, k**). Data are mean \pm s.d. Scale bars: 20 μ m (**c, f**), 50 μ m (**h, j**), 5 mm (**a**, top), 100 μ m (**a**, bottom). Schematic in **n** was created using BioRender.com.

spared the crypt areas (Extended Data Fig. 11g) where LGR5⁺ tumour stem-like cells reside. We performed immunofluorescence for $Lgr5$ -GFP and SOX17 and found that LGR5 and SOX17 were mutually exclusive (Fig. 5h). $Lgr5$ -GFP⁻ tumour cells, which were enriched for SOX17 expression (Fig. 5h), had significantly lower expression of MHC-I compared with $Lgr5$ -GFP⁺ tumour cells (Fig. 5i and Extended Data Fig. 11h). Given that in this model tumours initiated from LGR5⁺ intestinal stem cells and that the fraction of $Lgr5$ -GFP⁺ cells in tumours decreased over time (Extended Data Fig. 13a–c), this raises the possibility that SOX17 endows MHC-I^{low}LGR5⁻ immune-resistant tumour cells a selective advantage

compared with MHC-I^{hi}LGR5⁺ tumour cells. In transplantation assays, $Lgr5$ -GFP⁺ and $Lgr5$ -GFP⁻ cells from AKP tumours engendered tumours at similar frequencies and, regardless of the cell of origin, the tumours consisted of $Lgr5$ -GFP⁺SOX17⁻ cells and $Lgr5$ -GFP⁻SOX17⁺ cells, which is consistent with known plasticity between the $Lgr5$ -positive and $Lgr5$ -negative states in CRC^{31–33} (Extended Data Fig. 14a–f). Thus, we utilized autochthonous tumour models to test this hypothesis. *Sox17*-null, *Apc*-null tumours that developed in CD8⁺ T cell-depleted mice showed a significantly higher fraction of $Lgr5$ -GFP⁺ tumour cells compared with control *Apc*-null tumours (Fig. 5j,k). Similarly, when

Article

Sox17-proficient *Apc*-null tumours were depleted of CD8⁺ T cells, the fraction of *Lgr5*-GFP⁺ tumour cells significantly increased (Extended Data Fig. 13d–f). Together, these findings indicate that engagement of the SOX17 programme in adenoma cells drives the production of less immunogenic LGR5[−] tumour cells, which more effectively allows for immune evasion from CD8⁺ T cells.

SOX17 loss in AKP tumours also led to the upregulation of both *Lgr5* (Extended Data Fig. 13g) and MHC-I expression (Fig. 4f,g), whereas SOX17-OE tumours significantly decreased *Lgr5* expression and LGR5⁺ tumour cell numbers as detected by RT-qPCR and *in situ* hybridization (Extended Data Fig. 13h,i). Further validating that SOX17 directly regulates LGR5 expression, CUT&RUN analysis revealed that SOX17 directly binds to the promoter and introns of *Lgr5* (Fig. 5i), indicating that SOX17 may function as a transcriptional repressor for LGR5. A hallmark of the fetal intestinal gene expression programme is downregulation of LGR5 (refs. 18–20), a gene signature that was strongly induced in primary tumour-derived AKP organoids where SOX17 was highly expressed (Fig. 1c). Since SOX17 distinguishes fetal stem cells from their adult counterparts^{34,35}, we assessed whether enforced SOX17 expression reactivated this gene programme in AKP organoids. GSEA revealed that SOX17-OE activated this fetal intestinal gene expression signature (that is, upregulation of FETAL_SPHEROID_UP genes and downregulation of FETAL_SPHEROID_DOWN genes) whereas SOX17-null tumours repressed it (Fig. 5m). Collectively, our results demonstrate that SOX17 mediates *in vivo* epigenetic reprogramming of tumours, producing LGR5[−] cells that repress IFNγ signalling and facilitates immune evasion in early colon tumorigenesis (Fig. 5n and Supplementary Fig. 5).

Discussion

A hallmark of cancer is its ability to escape from immune clearance. Although it is a crucial step during tumorigenesis, very little is known about how pre-cancerous lesions evade recognition by the immune system. In the intestine, LGR5⁺ stem cells initiate most pre-malignant adenomas from which CRC arises¹. We previously demonstrated that LGR5⁺ stem cells are susceptible to T cell-mediated immune surveillance³⁶. The underpinnings that enable the transition of these cells from immune-susceptible to resistant upon acquisition of oncogenic mutations to allow cancer growth has not been explored. Here we reveal that tumour-initiating cells in the intestine acquire a fetal programme that blocks LGR5 expression, allowing a switch from immunogenic LGR5⁺ cells to immune-silent LGR5[−] cells (Fig. 5n). Since embryonic and fetal cells are less immunogenic than adult cells³⁷ and can even display some immune privilege³⁸, our results indicate that early pre-cancerous colon cells may hijack a fetal programme to evade cellular immunity.

This early pro-tumorigenic fetal programme is orchestrated by SOX17—a transcription factor that is required for endodermal development^{11–13} and is silenced in healthy adult intestinal epithelium. We found that during the initial stages of tumorigenesis, SOX17 is re-expressed in pre-cancerous colonic epithelial cells in both mouse and human adenomas (Extended Data Figs. 11d and 12a). Its deletion prevented adenoma formation in *Lgr5*^{creERT2},*Apc*^{fl/fl} mice and tumour development in organoid-derived CRCs implanted in immunocompetent mice (Figs. 2d–g and 5a,b). In both mouse models—genetically engineered mice and CRC organoid transplantation—depletion of CD8⁺ T cells was sufficient to rescue the ability of SOX17-deficient tumour cells to grow (Figs. 3h–j and 5f,g). Thus, the revival of this SOX17 fetal programme upon tumour initiation constitutes a key step in colon cancer initiation by suppressing anti-tumour immunity.

Mechanistically, SOX17 downregulates the expression of the receptor for IFNγ (IFNGR1) and, consequently, dampens the ability of colon cancer cells to respond to this key cytokine. In line with this, multiple studies have shown the relevance of IFNγ signalling for successful

anticancer immune responses. For example, *in vivo* CRISPR–Cas9 screens have demonstrated that impairment of the IFNγ signalling cascade undermines the response to immunotherapy^{27,39,40}. Accordingly, loss-of-function mutations in the IFNγ receptor pathway have been associated with resistance to immune checkpoint blockade in patients^{41,42}. Although genomic defects in the IFNγ pathway have frequently been found in cancer, here we identify—to our knowledge—the first mechanistic evidence of a pro-tumorigenic transcriptional regulator that directly blunts the expression of the IFNγ receptor itself. Moreover, whereas mutations in the IFNγ-sensing pathway accumulate in cancers over time owing to immunoediting, our work reveals a transcriptional downregulation of *Ifngr1* that occurs at the earliest stages of tumour development. Decreasing the amount of receptors for IFNγ constitutes an effective strategy for immune evasion: (1) It abrogates the ability of tumour cells to upregulate MHC-I, thereby reducing recognition by CD8⁺ T cells; and (2) it dampens secretion of crucial T cell attractant chemokines such as CXCL10, which prevents T cell recruitment. Thus, by decreasing IFNγ sensing, SOX17 collectively impairs several key steps in anti-tumour adaptive immunity. An early reduced ability of tumour cells to respond to IFNγ thwarts immune recognition at a vulnerable period of tumour development before the protective immune-suppressive microenvironment of an advanced cancer is established. In agreement with this notion, histopathological analysis of human adenoma showed that all samples were SOX17^{hi/mid} (Extended Data Fig. 12a,b). As tumours evolve and an immune-suppressive microenvironment is established, this suppressive milieu may be able to sustain itself by creating complex immune hubs¹⁴³. Thus, whereas SOX17 is essential at the earliest stages of tumorigenesis, it may be less critical in advanced disease. This may explain how around 20% of the analysed advanced primary CRC specimens displayed negative or low signals of SOX17 positivity (Extended Data Fig. 12c,d). Previous studies have identified SOX17 both as a tumour suppressor gene^{44–46} and as an oncogene^{47,48}, suggesting a tumour stage- and organ-context-dependent role of SOX17.

Finally, future work will be required to explain the role of SOX17 at later stages of CRC, including when tumours metastasize to distant organs. Another important question to be addressed in the future is the mechanisms whereby SOX17 expression is induced *in vivo* at the beginnings of tumorigenesis. In summary, our work reveals the essential role of a recalled fetal programme in nascent tumours in the intestine that permits cancer development by blunting IFNγ sensing and facilitating escape from adaptive immunity.

Online content

Any methods, additional references, Nature Portfolio reporting summaries, source data, extended data, supplementary information, acknowledgements, peer review information; details of author contributions and competing interests; and statements of data and code availability are available at <https://doi.org/10.1038/s41586-024-07135-3>.

1. Pelka, K. et al. Spatially organized multicellular immune hubs in human colorectal cancer. *Cell* **184**, 4734–4752.e4720 (2021).
2. Lin, J. R. et al. Multiplexed 3D atlas of state transitions and immune interaction in colorectal cancer. *Cell* **186**, 363–381.e319 (2023).
3. Tauriello, D. V. F. et al. TGFβ drives immune evasion in genetically reconstituted colon cancer metastasis. *Nature* **554**, 538–543 (2018).
4. Shankaran, V. et al. IFNγ and lymphocytes prevent primary tumour development and shape tumour immunogenicity. *Nature* **410**, 1107–1111 (2001).
5. Koebel, C. M. et al. Adaptive immunity maintains occult cancer in an equilibrium state. *Nature* **450**, 903–907 (2007).
6. Beyaz, S. et al. Dietary suppression of MHC class II expression in intestinal epithelial cells enhances intestinal tumorigenesis. *Cell Stem Cell* **28**, 1922–1935.e1925 (2021).
7. Roper, J. et al. *In vivo* genome editing and organoid transplantation models of colorectal cancer and metastasis. *Nat. Biotechnol.* **35**, 569–576 (2017).
8. Roper, J. et al. Colonoscopy-based colorectal cancer modeling in mice with CRISPR–Cas9 genome editing and organoid transplantation. *Nat. Protoc.* **13**, 217–234 (2018).
9. Barker, N. et al. Crypt stem cells as the cells-of-origin of intestinal cancer. *Nature* **457**, 608–611 (2009).

10. Goto, N. et al. Lymphatics and fibroblasts support intestinal stem cells in homeostasis and injury. *Cell Stem Cell* **29**, 1246–1261.e1246 (2022).
11. Spence, J. R. et al. Sox17 regulates organ lineage segregation of ventral foregut progenitor cells. *Dev. Cell* **17**, 62–74 (2009).
12. Shviddasani, R. A. Molecular regulation of vertebrate early endoderm development. *Dev. Biol.* **249**, 191–203 (2002).
13. Kanai-Azuma, M. et al. Depletion of definitive gut endoderm in Sox17-null mutant mice. *Development* **129**, 2367–2379 (2002).
14. Schepers, A. G. et al. Lineage tracing reveals Lgr5⁺ stem cell activity in mouse intestinal adenomas. *Science* **337**, 730–735 (2012).
15. The Cancer Genome Atlas Network. Comprehensive molecular characterization of human colon and rectal cancer. *Nature* **487**, 330–337 (2012).
16. Westcott, P. M. K. et al. Low neoantigen expression and poor T-cell priming underlie early immune escape in colorectal cancer. *Nat. Cancer* **2**, 1071–1085 (2021).
17. Heide, T. et al. The co-evolution of the genome and epigenome in colorectal cancer. *Nature* **611**, 733–743 (2022).
18. Fordham, R. P. et al. Transplantation of expanded fetal intestinal progenitors contributes to colon regeneration after injury. *Cell Stem Cell* **13**, 734–744 (2013).
19. Mustata, R. C. et al. Identification of Lgr5-independent spheroid-generating progenitors of the mouse fetal intestinal epithelium. *Cell Rep.* **5**, 421–432 (2013).
20. Nusse, Y. M. et al. Parasitic helminths induce fetal-like reversion in the intestinal stem cell niche. *Nature* **559**, 109–113 (2018).
21. Llosa, N. J. et al. The vigorous immune microenvironment of microsatellite instable colon cancer is balanced by multiple counter-inhibitory checkpoints. *Cancer Discov.* **5**, 43–51 (2015).
22. Beltra, J. C. et al. Developmental relationships of four exhausted CD8⁺ T cell subsets reveals underlying transcriptional and epigenetic landscape control mechanisms. *Immunity* **52**, 825–841.e828 (2020).
23. Miller, B. C. et al. Subsets of exhausted CD8⁺ T cells differentially mediate tumor control and respond to checkpoint blockade. *Nat. Immunol.* **20**, 326–336 (2019).
24. Khan, O. et al. TOX transcriptionally and epigenetically programs CD8⁺ T cell exhaustion. *Nature* **571**, 211–218 (2019).
25. Di Pilato, M. et al. CXCR6 positions cytotoxic T cells to receive critical survival signals in the tumor microenvironment. *Cell* **184**, 4512–4530.e4522 (2021).
26. Ikeda, H., Old, L. J. & Schreiber, R. D. The roles of IFN γ in protection against tumor development and cancer immunoediting. *Cytokine Growth Factor Rev.* **13**, 95–109 (2002).
27. Pan, D. et al. A major chromatin regulator determines resistance of tumor cells to T cell-mediated killing. *Science* **359**, 770–775 (2018).
28. Miao, D. et al. Genomic correlates of response to immune checkpoint blockade in microsatellite-stable solid tumors. *Nat. Genet.* **50**, 1271–1281 (2018).
29. Reschke, R. & Gajewski, T. F. CXCL9 and CXCL10 bring the heat to tumors. *Sci. Immunol.* **7**, eabq6509 (2022).
30. Fearon, E. R. & Vogelstein, B. A genetic model for colorectal tumorigenesis. *Cell* **61**, 759–767 (1990).
31. Shimokawa, M. et al. Visualization and targeting of LGR5⁺ human colon cancer stem cells. *Nature* **545**, 187–192 (2017).
32. de Sousa e Melo, F. et al. A distinct role for Lgr5⁺ stem cells in primary and metastatic colon cancer. *Nature* **543**, 676–680 (2017).
33. Fumagalli, A. et al. Plasticity of Lgr5-negative cancer cells drives metastasis in colorectal cancer. *Cell Stem Cell* **26**, 569–578.e567 (2020).
34. He, S., Kim, I., Lim, M. S. & Morrison, S. J. Sox17 expression confers self-renewal potential and fetal stem cell characteristics upon adult hematopoietic progenitors. *Genes Dev.* **25**, 1613–1627 (2011).
35. Kim, I., Saunders, T. L. & Morrison, S. J. Sox17 dependence distinguishes the transcriptional regulation of fetal from adult hematopoietic stem cells. *Cell* **130**, 470–483 (2007).
36. Agudo, J. et al. Quiescent tissue stem cells evade immune surveillance. *Immunity* **48**, 271–285.e275 (2018).
37. Drukker, M. et al. Human embryonic stem cells and their differentiated derivatives are less susceptible to immune rejection than adult cells. *Stem Cells* **24**, 221–229 (2006).
38. Li, L. et al. Human embryonic stem cells possess immune-privileged properties. *Stem Cells* **22**, 448–456 (2004).
39. Manguso, R. T. et al. In vivo CRISPR screening identifies *Ptpn2* as a cancer immunotherapy target. *Nature* **547**, 413–418 (2017).
40. Patel, S. J. et al. Identification of essential genes for cancer immunotherapy. *Nature* **548**, 537–542 (2017).
41. Gao, J. et al. Loss of IFN γ pathway genes in tumor cells as a mechanism of resistance to anti-CTLA-4 therapy. *Cell* **167**, 397–404.e399 (2016).
42. Zaretsky, J. M. et al. Mutations Associated with acquired resistance to PD-1 blockade in melanoma. *N. Engl. J. Med.* **375**, 819–829 (2016).
43. Baldominos, P. et al. Quiescent cancer cells resist T cell attack by forming an immunosuppressive niche. *Cell* **185**, 1694–1708.e1619 (2022).
44. Zhang, W. et al. Epigenetic inactivation of the canonical Wnt antagonist SRY-box containing gene 17 in colorectal cancer. *Cancer Res.* **68**, 2764–2772 (2008).
45. Wang, L. et al. SOX17 antagonizes the WNT signaling pathway and is epigenetically inactivated in clear-cell renal cell carcinoma. *Oncotargets Ther.* **14**, 3383–3394 (2021).
46. Wang, M. et al. Loss-of-function mutations of SOX17 lead to YAP/TEAD activation-dependent malignant transformation in endometrial cancer. *Oncogene* **42**, 322–334 (2023).
47. Delgiorno, K. E. et al. Identification and manipulation of biliary metaplasia in pancreatic tumors. *Gastroenterology* **146**, 233–244.e235 (2014).
48. Tan, D. S., Holzner, M., Weng, M., Srivastava, Y. & Jauch, R. SOX17 in cellular reprogramming and cancer. *Semin. Cancer Biol.* **67**, 65–73 (2020).

Publisher's note Springer Nature remains neutral with regard to jurisdictional claims in published maps and institutional affiliations.

Springer Nature or its licensor (e.g. a society or other partner) holds exclusive rights to this article under a publishing agreement with the author(s) or other rightsholder(s); author self-archiving of the accepted manuscript version of this article is solely governed by the terms of such publishing agreement and applicable law.

© The Author(s), under exclusive licence to Springer Nature Limited 2024

Article

Methods

Mice

Mice were under the husbandry care of the Department of Comparative Medicine in the Koch Institute for Integrative Cancer Research. All procedures were conducted in accordance with the American Association for Accreditation of Laboratory Animal Care and approved by MIT's Committee on Animal Care. *Lgr5-2A-EGFP-2A-creERT2* (ref. 10), *Lgr5-EGFP-ires-creERT2* (ref. 49), *Villin-creERT2* (ref. 50), *Sox17^{f/f}* (ref. 11), *Apc^{f/f}* (ref. 51), *Kras^{LSL-G12D}* (ref. 52), *Trp53^{f/f}* (ref. 53), *OT-1* (ref. 54), *Rosa26-Cas9-2A-EGFP^{ss}* and *Rosa26-LSL-tdTomato⁵⁶* mice were maintained on a C57BL/6 background. Orthotopic transplantation experiments with C57BL/6 organoids were performed on syngeneic C57BL/6, *Rosa26-Cas9-2A-EGFP*, and *Rag2^{-/-}* (ref. 57) recipient mice. Orthotopic transplantation experiments with human AKP organoids were performed on *NOD-Prkdc^{em26Cds2}Il2rg^{em26Cds22}/NjUcr1* (NCG) recipient mice obtained from Charles River. In this study, both male and female mice were used at the age of 8–12 weeks. For induction of Cre-mediated recombination, 100 µl of 20 mg ml⁻¹ tamoxifen (MedChem Express, HY-13757A) in corn oil were injected intraperitoneally over 4 consecutive days. Doxycycline was administered via food pellets⁵⁸ (625 mg kg⁻¹) (Harlan Teklad, TD.09628).

Mouse colonoscopy and mucosal injection

Colonoscopy was performed using the Image 1 H3-Z Spies HD Camera System (part TH100), Image 1 HUB CCU (parts TC200, TC300), 175 W D-Light Cold Light Source (part 20133701-1), AIDA HD capture system, and Hopkins Telescope (part 64301AA)⁷. For orthotopic organoid transplants, organoids were dissociated by TrypLE Express (Thermo Fisher Scientific) for 10 min at 37 °C, passed through a 100-µm filter, resuspended in basal medium (Advanced DMEM supplemented with, penicillin/streptomycin (Corning) and GlutaMAX (Thermo Fisher Scientific)) with 5% FBS, 10% Matrigel (Corning), and 10 µM Y-27632 (APEX BIO, A3008) supplementation, and then transplanted to the colon mucosa of recipient mice (8–12 weeks old) by colonoscopy⁷⁸ or direct mucosal injection³². For colonoscopy-guided injection, a custom injection needle (Hamilton, 7803-05), a syringe (Hamilton, 7656-01), a transfer needle (Hamilton, 7770-02), and a colonoscope with integrated working channel (Richard Wolf 1.9 mm/9.5 French paediatric urethroscope, 8626.431) were used. For direct mucosal injection, 29G insulin syringes (BD, 324702) were used. For each injection, 50 µl of medium containing 75,000 organoid cells was injected. Tumours were collected at 1–6 weeks post-transplantation, and bright light and fluorescent images of the tumours were captured using Nikon SMZ18 Stereo Microscope. To quantify the tumour size, tdTomato⁺ areas in the images were calculated using ImageJ Version 2.9.0/1.53t as previously described⁷. For mucosal delivery of 4-OH-tamoxifen (MedChem Express, 68047-06-3) in the autochthonous tumour models, 50 µl of PBS containing 100 µM 4-OH-tamoxifen was injected by colonoscopy^{78,59}.

Organoid generation and culture

Mouse naive AKP organoids were embedded in Matrigel and cultured in 5% FBS + basal medium (Advanced DMEM supplemented with penicillin/streptomycin and GlutaMAX). To generate *in vivo* tumour-derived AKP organoids, tumours were collected from the transplantation mice, minced using surgical scissors, and digested in a digestion buffer containing 500 U ml⁻¹ Collagenase Type 1 (Worthington, LS004196) at 37 °C for 40 min with gentle agitation. Cells were washed, filtered through a 100-µm filter, centrifuged for 5 min at 300g. Cells were embedded in Matrigel and cultured in 5% FBS + basal medium. These organoids were passaged 4–6 times until only tdTomato⁺ cancer cells were present in the culture and then used for further analyses or frozen in FBS containing 10% DMSO for the later use.

Human AKP organoids were embedded in Matrigel and cultured in ENAS medium (Advanced DMEM supplemented with 50 ng ml⁻¹ EGF

(PeproTech, 315-09), 100 ng ml⁻¹ Noggin (PeproTech, 250-38), 500 nM A83-01 (Tocris, 2939), 10 µM SB202190 (Sigma-Aldrich, S7067), 1 mM N-acetyl-L-cysteine (Sigma-Aldrich, A7250), 10 nM human gastrin I (Sigma-Aldrich, G9020), B27 (Thermo Fisher Scientific, 17504044), penicillin/streptomycin and GlutaMAX) as previously described⁶⁰.

CRISPR–Cas9-mediated gene editing of organoids

To generate mouse naive AKP colon organoids, colon organoids from *Kras-LSL-G12D;Trp53 fl/fl; Rosa26-LSL-tdTomato* mice were cultured in L-WRN medium⁶¹, transfected with pSECC plasmid (containing Cre, Cas9 and U6 promoter for sgRNA, Addgene, #60820) carrying sgApc (5'-GTCTGCCATCCCTTCACGTT-3') by spinoculation using Lipofectamine 2000 (Thermo Fisher Scientific, 11668027)⁶², and then selected in medium without WNT3A or R-spondin-1 supplemented with 10 µM nutlin-3 (Sigma-Aldrich, N6287).

To generate human naive AKP colon organoids^{63,64}, first, normal colonic organoids from the patients were generated and cultured in the L-WRN medium. Normal colonic organoids were transfected with pX330 plasmid (Addgene, #60820) carrying sgAPC (5'-GTTTG AGCTGTTGAGGAGG-3') by spinoculation using lipofectamine 2000, and selected in medium without WNT3A or R-spondin-1 to establish *APC^{-/-}* organoids. Single-cell-derived organoids were picked and expanded, and clones with the biallelic frameshift mutations confirmed by Sanger sequencing were selected. Then, *APC^{-/-}* organoids were transfected with pX330 plasmid (Addgene, #60820) carrying sgTP53 (5'-GGGCAGCTACGGTTCCGTC-3'), and selected in medium without WNT3A or R-spondin-1 supplemented with 10 µM nutlin-3 (Sigma-Aldrich, N6287). Single-cell-derived organoids were picked and expanded, and clones with the biallelic frameshift mutations were selected. These *APC^{-/-};TP53^{-/-}* organoids were transfected with pX330 plasmid (#60820) carrying sgKRAS (5'-GTAGTTGGAGCTGGTGGCGT-3') and a targeting vector harbouring a G12D point mutation with neomycin resistant cassette flanked by *loxP* sites in the intron, and selected by 400 µg ml⁻¹ G418 (Sigma-Aldrich, G8168). Then, organoids were transduced with Ad5-CMV-Cre-eGFP (UI Viral Vector Core, 1174) to excise the neomycin resistant cassette flanked by *loxP* sites. Three days after the transduction, single GFP⁺ cells were sorted and cultured for expansion. Sanger sequencing was performed to confirm the correct G12D point mutation.

To knockout *Sox17* in mouse AKP organoids, sgRNAs for *Sox17* (guide 1: 5'-CGAGACTGGAGCGTAAGTGT-3', guide 2: 5'-GCCGGCGC GCTTGGTCCCCGA-3') were cloned into LentiCRISPRv2 (Addgene, #52961). For lentivirus production⁶⁵, 10 µl of Lipofectamine 2000 reagent in 250 µl Opti-MEM medium (Thermo Fisher Scientific, 31985062) and a total of 4 µg of DNA (2 µg of lentiviral backbone constructs, 1 µg of pSpax2 (Addgene, #12260), and 1 µg of pMD2.G (Addgene, #12259)) in 250 µl Opti-MEM medium were mixed together, incubated for 15 min, and added to 293T cells cultured in 6-well plates. Culture medium was changed the next day. The supernatant was collected 48 h after the medium change, and passed through a 0.45-µm filter. For lentivirus transduction, organoids were dissociated by incubation with TrypLE Express for 5 min at 37 °C, transduced with the lentivirus supernatant by spinoculation at 600g at 32 °C for 60 min in a 48-well culture plate, and incubated for another 4 h in an incubator at 37 °C as previously reported⁶⁵. Organoids were then embedded in Matrigel and cultured in 5% FBS + basal medium. Two days after transduction, culture medium was changed to 5% FBS + basal medium plus 8 µg ml⁻¹ puromycin (Invivogen, ant-pr-1). After 10–14 days, single-cell-derived organoids were picked and expanded, and clones with the biallelic frameshift mutations confirmed by Sanger sequencing were selected. Western blotting was performed to confirm the SOX17 knockout at the protein level. For the generation of control organoids, sgScramble (5'-AAAATGCGGATACAATCAG-3') was used for the analogous methods. Multiple clones for SOX17-KO and control lines were established for further analysis as shown in Extended Data Fig. 4c.

To knock out *Ifngr1*, *H2k1*, *B2m* and *Cxcl10* in SOX17-KO organoids, sgRNAs for *Ifngr1* (5'-CGACTTCAGGGTGAATACG-3'), *H2k1* (5'-CGAG ATATGAGCCCGGGCG-3'), *B2m* (5'-AGTATACTCACGCCACCA C-3') and *Cxcl10* (5'-AGCGGACCGTCCTGCGAGA-3') were cloned into LentiCRISPRv2 neo (Addgene, #98292) and the analogous methods (except that organoids were selected by 400 µg ml⁻¹ G418 (Sigma-Aldrich, G8168)) were used to establish the knockout clones.

Establishment of SOX17 overexpression and knockdown plasmids and organoids

For constitutive SOX17 overexpression, mouse *Sox17* sequence was amplified by PCR from FUW-TetO-SOX17 plasmid (Addgene, #128828) to have overlapping DNA ends with the donor EF-1a-spCas9-T2A-mNeonGreen-P2A-puro vector (Addgene, #122183). spCas9 sequence of the donor EF-1a-spCas9-T2A-mNeonGreen-P2A-puro vector was cut by restriction enzymes and replaced with mouse SOX17 sequence using In-Fusion HD Cloning Kit (Clontech, 638916) following the manufacturer's protocol. The EF-1a-SOX17-T2A-mNeonGreen-P2A-puro vector is introduced into AKP organoids by lentivirus transduction (described above) and the organoids were selected by 8 µg ml⁻¹ puromycin. Then, organoids with stable expression of mNeonGreen fluorescence were picked and expanded for further analyses. Overexpression of SOX17 at the protein level was confirmed by Western blotting.

For doxycycline-inducible SOX17 overexpression, PGK-neo sequence was amplified by PCR from PGK-neo-lox2-DTA.2 plasmid (Addgene, #13449) and incorporated into FUW-TetO-*Sox17* vector using In-Fusion HD Cloning Kit. First, pLenti-CMV-rtTA3-Hygro vector (Addgene, #26730) was introduced to AKP organoids by lentivirus transduction and the organoids were selected by 500 µg ml⁻¹ hygromycin (Thermo Fisher Scientific, 10687010). Then, FUW-TetO-*Sox17*-PGK-neo vector was introduced to the organoids by lentivirus transduction and the organoids were selected by 8 µg ml⁻¹ puromycin. Overexpression of SOX17 at the protein level was confirmed by Western blotting 72 h after the administration of 1 µg/m doxycycline to the culture medium (Sigma-Aldrich, D9891).

For doxycycline-inducible *Sox17* knockdown, shRNA targeting *Sox17* (5'-TTTAAACAAAAATCTCGTGA-3')⁶⁶ was incorporated into LT3GE-PIR plasmid (Addgene, #111177) as previously described^{67,68}. LT3GEPIR carrying shRenilla (control vector) was kindly provided by L. E. Dow. These vectors were introduced into AKP organoids by lentivirus transduction (described above) and the organoids were selected by 8 µg ml⁻¹ puromycin. *Sox17* knockdown was confirmed by RT-qPCR 48 h after the administration of 1 µg ml⁻¹ doxycycline to the culture medium.

Human samples

All human samples were collected from patients at Massachusetts General Hospital (MGH) under protocols approved by the Institutional Review Board (IRB) at MGH and the Massachusetts Institute of Technology Committee on the Use of Humans as Experimental Subjects. For human organoid generation, Informed consent was obtained from all subjects, and 0.5–1 cm³ portions of fresh normal colonic epithelium was dissected from grossly normal colon in patients undergoing CRC surgery at MGH, with the specimen taken >10 cm from any grossly apparent mass. Endoscopically resected human colonic sections that were diagnosed as adenomas were obtained from 8 patients with familial adenomatous polyposis (FAP) and 11 patients without FAP. Surgically resected human colonic sections that were diagnosed as CRCs at different pathologic tumour stages (pT1–pT4) were obtained from 39 patients. All samples were treatment-naïve (without neoadjuvant therapy).

Immunohistochemistry and immunofluorescence

Tissues were fixed in 10% formalin, paraffin embedded and sectioned in 4- to 5-µm sections as previously described^{69–71}. Antigen retrieval was performed using Borg Decloaker RTU solution (Biocare Medical,

BD1000G1) or citrate buffer with a pressurized Decloaking Chamber (Biocare Medical, NxGen). Antibodies and respective dilutions used for immunohistochemistry are as follows: goat polyclonal anti-SOX17 (1:200, R&D, AF1924), rabbit monoclonal anti-SOX17 (1:2,000, abcam, ab224637), mouse monoclonal anti-β-catenin (1:50, BD Biosciences, 610154), rabbit monoclonal anti-CD4 (1:400, abcam, ab183685), rabbit monoclonal anti-CD8 (1:1000, abcam, ab217344), mouse monoclonal anti-CD8 (1:100, abcam, ab17147), rat anti-BrdU (1:2,000, abcam, ab6326), and mouse anti-Ki67 (1:400, BD, 550609). Biotin-conjugated secondary donkey anti-rabbit, anti-goat, anti-rat, or anti-mouse antibodies were used (1:500, Jackson ImmunoResearch). Vectastain Elite ABC immunoperoxidase detection kit (Vector Laboratories, PK6100) was followed by Signalstain DAB substrate kit for visualization (CST, 8049 S). All antibody dilutions were performed in Signalstain Antibody Diluent (CST, 8112L). The following primary antibodies were used for immunofluorescence: rabbit monoclonal anti-Phospho-Stat1 (1:400, Cell Signaling, 9167), rabbit monoclonal anti-SOX17 (1:2,000, abcam, ab224637), and goat polyclonal anti-GFP (1:500, abcam, ab6673). Alexa Fluor secondary antibodies, anti-goat 488, anti-rabbit 488, anti-goat 568, anti-rabbit 568 (1:500, Thermo Fisher Scientific), were used for visualization. Slides were stained with Hoechst for 10 min and covered with Prolong Gold (Life Technologies, P36930) mounting medium. Images were acquired using a Nikon Eclipse 90i upright microscope equipped with a Hamamatsu Orca-ER CCD camera, and APC line 1200 light source. *Lgr5*-GFP+ areas were calculated using ImageJ version 2.9.0/1.53t. Beta-catenin+ tumour areas were determined by the areas of cells with positive nuclear staining for beta-catenin and were calculated using ImageJ Version 2.9.0/1.53t. Cell counts for SOX17+, BrdU+, Ki67+, pSTAT1+, CD4+ and CD8+ cells were conducted by researchers who were blinded to the genotype or treatment groups. SOX17+, BrdU+, Ki67+ and pSTAT1+ cells were determined by positive staining in the nucleus; CD4+ and CD8+ cells were determined by positive staining in the cell membrane.

Immunoblotting

Organoids are washed twice with PBS and resuspended in RIPA buffer (Cell Signaling Technology, 9806 S), incubated at 4 °C for 10 min, and centrifuged at 300g for 10 min. Supernatant was collected and boiled for 5 min. Lysates were loaded per sample onto a 4%–12% gradient gel, transferred on to PVDF membrane (Immobilon-P transfer, Millipore, ipvh00010) and incubated with goat polyclonal anti-SOX17 (1:200, R&D, AF1924) and mouse monoclonal anti-actin (1:1,000, Sigma-Aldrich, MAB1501) at 4 °C overnight. The membrane was washed and incubated with anti-goat IgG-HRP (1:5,000, Santa Cruz Biotechnology, sc-2056) and anti-mouse IgG-HRP (1:5,000, CST, 7076 S) at room temperature for 1 h. Signal is detected using Advansta WesternBright Sirus ECL detection kit (K12043D20) (Supplementary Fig. 1).

CD8+ or CD4+ T cell depletion, IFNAR1 blockade, and IFNy neutralization

To deplete CD8+ or CD4+ T cells, 200 µg of anti-CD8α (BioXcell, BE0061) or anti-CD4 (BioXcell, BE0003-1) in PBS was intraperitoneally injected twice a week, respectively. Antibody injection was initiated 2 days before the organoid transplantation. For control, IgG isotype antibody (BioXcell, BE0090) was injected. For IFNAR1 blockade, 500 µg of anti-IFNAR1 (BioXcell, BE0241) in PBS was intraperitoneally injected one day before the organoid transplantation and then 250 µg of anti-IFNAR1 was injected every other day. For neutralization of IFNy, 250 µg of anti-IFNy (BioXcell, BE0055) in PBS was intraperitoneally injected one day before the organoid transplantation and then every other day thereafter. For control, isotype IgG1 antibody (BioXcell, BE0083) was injected.

Tissue preparation for T cell flow cytometry

Colon tumours were collected under the fluorescent microscope, minced using surgical scissors, and digested in a digestion buffer

Article

containing 500 U ml⁻¹ Collagenase Type 1 and 20 µg ml⁻¹ DNase (Roche, 10104159001) at 37 °C for 40 min with gentle agitation. Tumours were then further dissociated with a gentleMACS Octo Dissociator (Miltenyi Biotec) on the tumour _imp1.1 setting, filtered through a 100-µM filter, and centrifuged for 5 min at 2,000 rpm. To isolate lymphocytes⁷², cells were resuspended in 5 ml 44% percoll, underlaid with 2 ml 67% percoll, centrifuged at 2,000 rpm for 20 min with no brake. Buffy coat at the interface was isolated using a Pasteur pipette, resuspended in RPMI-1640 + 5% FBS, and centrifuged at 2,000 rpm for 10 min. For cytokine staining, these lymphocytes were then cultured in T cell medium (RPMI-1640 with 10% FBS, 20 mM HEPES, 1 mM sodium pyruvate, 2 mM L-glutamine, 50 µM β-mercaptoethanol, 1× non-essential amino acids and penicillin/streptomycin) with dGolgiPlug (1:1,000, BD, 555029) and 2 µM Monensin Solution (BioLegend, 420701) for 3 h at 37 °C. Cells were washed and live/dead staining with Fixable Viability Dye eFluor 780 (Thermo Fisher Scientific, 65-0865-14) and cell surface stains were performed. Cells were fixed for 1 h at room temperature in Fixation/Permeabilization Concentrate (Thermo Fisher Scientific, 00-5123-43) diluted 1:3 in Fixation/Permeabilization diluent (Thermo Fisher Scientific, 00-5223-56) and washed in permeabilization buffer (Thermo Fisher Scientific, 00-8333-56). Intracellular staining was performed in permeabilization buffer overnight at 4 °C. Cells were washed and resuspended in FACS buffer for analysis on a BD LSRFortessa four-laser, 18-colour flow cytometer. The data were analysed using FlowJo software (version 10, TreeStar) and FACSDiva software (version 8.0, BD Biosciences). Single lymphocytes were gated on FSC-A versus SSC-A, FSC-H versus FSC-W, and SSC-H versus SSC-W. Live CD8⁺ T cells were gated on positive CD8α and negative Fixable Viability Dye eFluor 780 staining.

OT-1 T cell activation and organoid co-culture

Co-culture experiments of organoids and activated OT-1 T cells were performed as described¹⁶. Spleen and lymph nodes from OT-1 mice were collected in PBS. Red blood cells were lysed by ACK lysing buffer (Lonza, 10-548E). Cells were resuspended in T cell medium (described above) + 10 ng ml⁻¹ human IL-2 (PeproTech, 200-02) and 1 µM SIINFEKL peptide (Anaspec, AS-60193-1), counted and plated at 1 × 10⁶ cells per ml. Stimulation was performed for 24 h at 37 °C. CD8⁺ T cells were then purified using the CD8a⁺ T Cell Isolation kit (Miltenyi Biotech, 130-104-075) and expanded in T cell medium + human IL-2 with daily splitting. At day 3, organoids and OT-1s were plated at 1:1 ratio at 5,000 organoid single cells in 60 µl Matrigel. Co-cultures were plated in triplicate at 20 µl per dome, grown in minimal medium (Advanced DMEM supplemented with B27, penicillin/streptomycin, GlutaMAX) + 10 ng ml human IL-2.

RNA extraction and RNA-seq library preparation

RNA was extracted from organoids using TRIzol and Ambion PureLink RNA Mini Kit (Thermo Fisher Scientific, 12-183-018 A) according to the manufacturer's instructions. For RNA-seq library preparation, NEBNext Ultra II Directional RNA preparation with poly(A) selection is used to selectively capture mRNA from total RNA and barcoded libraries were generated. 2 × 40 paired-end sequencing was performed on an Illumina NextSeq 500.

RT-qPCR and in situ hybridization

RNA was converted to cDNA using qScript cDNA SuperMix (Quantabio, 95048-100). RT-qPCR reactions were performed using cDNA with SYBR green fast mix (Quantabio, PerfeCTa, 95072-012) on a Roche lightcycler (Roche, LightCycler 480 II). The following primers used for RT-qPCR: mouse *Gapdh* forward, 5'-AGGTCGGTGTGAACGGATTG-3'; mouse *Gapdh* reverse, 5'-TGTAGACCATGTAGTTGAGGTCA-3'; mouse *Lgr5* forward, 5'-TCCTAGAAGAGTTACGTCTTGCT-3'; mouse *Lgr5* reverse, 5'-CCTTGGGAATGTGTCAAAGC-3'; mouse *Ifng1* forward, 5'-CTGGCAGGATATTCTGCTGG-3'; mouse *Ifngr1* reverse, 5'-GCA TACGACAGGGTTCAAGTTAT-3'; human *GAPDH* forward, 5'-GGAG

CGAGATCCCTCCAAAAT-3'; human *GAPDH* reverse, 5'-GGCTGTT GTCATACTTCTCATGG-3'; human *SOX17* forward, 5'-CTCCGGTGT GAATCTCCCC-3'; human *SOX17* reverse, 5'-CACGTCAGGATACTTG CAGTAAT-3'.

Single-molecule in situ hybridization was performed using Advanced Cell Diagnostics RNAscope 2.5 HD Detection Kit. The in situ hybridization probes used in this study are as follows: Mm-*Cxcl10* (Ref 408921), Mm-*Lgr5* (Ref 312171).

ATAC-seq library preparation

ATAC-seq was performed on organoids as previously described⁷³. In brief, organoids were dissociated by TrypLE Express for 10 min at 37 °C, passed through a 40-µm filter, and a total of 50,000 cells were centrifuged and washed twice with PBS. Cells were resuspended in 50 µl of buffer with TDE1 enzyme (10 mM tris-HCl (pH 7.5), 5 mM MgCl₂, 30% PBS, 0.1% NP-40 (Sigma-Aldrich, 11332473001), 5% dimethylformamide, and Nextera Tn5 Transposase (Illumina, FC-121-1030) in H₂O) and incubated at 37 °C for 30 min with gentle agitation. DNA was isolated using the Qiagen MinElute PCR Purification Kit (QIAGEN, 28004). ATAC-seq libraries were PCR amplified using NEBNext High-Fidelity 2× PCR Master Mix (New England Biolabs, M0541S) for the appropriate numbers of cycles determined by RT-qPCR as previously described⁷³. The 2 × 75 paired-end sequencing was performed on an Illumina NextSeq 500.

CUT&RUN library preparation

CUT&RUN for SOX17 was performed using CUTANA CUT&RUN kit (EpiCypher, 14-1048) as previously described⁷⁴. In brief, concanavalin A-coated magnetic beads were activated by washing twice with bead activation buffer. In total, 5 × 10⁵ cells from organoids were washed twice and resuspended in wash buffer, and activated bead suspension was added to each sample. Samples were then incubated at room temperature for 10 min. The sample tubes were placed on a magnet stand, and the supernatant was removed. 50 µl of the antibody buffer (0.1% digitonin wash buffer and 2 mM EDTA) with 0.5 µl anti-SOX17 (R&D, AF1924) was then added to each sample and mixed. Samples were incubated at 4 °C overnight. The sample tubes were then placed on a magnet stand, and the supernatant was removed. The beads were washed twice with 0.1% digitonin wash buffer and resuspended in 50 µl 0.1% digitonin wash buffer. EpiCypher CUTANA pAG-MNase (2.5 µl) was added to each sample. Samples were incubated at room temperature for 10 min, placed on a magnet stand, and the supernatant was removed. The samples were washed twice with 0.1% digitonin wash buffer and resuspended in 50 µl of 0.1% digitonin wash buffer. 1 µl of 100 mM CaCl₂ was added to each sample and samples were incubated at 4 °C for 2 h. Stop buffer (33 µl) of was added to each sample and the samples were incubated at 37 °C for 10 min. The samples were placed on a magnet stand and the supernatant was collected to 1.5 ml tube. DNA was extracted using the CUTANA DNA Purification Kit. Libraries were prepared by NEB Ultra II Library Prep Kit for Illumina. Paired-end sequencing (2 × 40) was performed on an Illumina NextSeq 500.

RNA-seq data processing and differential expression analysis

Paired-end RNA-seq data from GSE222709 and GSE222710 were mapped to the UCSC mm9 mouse genome build (genome.ucsc.edu) using Bowtie⁷⁵ v2.2.6 and gene counts were quantified using RSEM⁷⁶ v1.2.12. Estimated expression counts generated by RSEM were upper quartile normalized to a count of 1,000 (ref. 77). Paired-end RNA-seq data from GSE245668 were used to quantify transcripts from the mm10 mouse assembly with the Ensembl version 101 annotation using Salmon version 1.3.0 (ref. 78) and gene level summaries were prepared using tximport version 1.16.1 (ref. 79). Differential expression analysis was done with DESeq2 version 1.30.1 (ref. 80) and differentially expressed genes were defined as those having an absolute aapeglm⁸¹ log₂ fold change greater than 1 and an adjusted P value less than 0.05. Mouse genes were mapped to human orthologues using Mouse Genome

Informatics (<http://www.informatics.jax.org/>) orthology report and preranked Gene Set Enrichment Analysis⁸² was done using GSEA version 4.0.3 with a custom gene set⁸³ or sets from MSigDB version 7.2 (ref. 84).

ATAC-seq data processing, differential expression analysis and motif analysis

Paired-end ATAC-seq reads were mapped to the UCSC mm9 mouse genome build (genome.ucsc.edu) using Bowtie⁷⁵ v2.2.6. To drop duplicate alignments, BAM files were processed with Picard MarkDuplicates v2.17.0 (<https://broadinstitute.github.io/picard/>). BAM files were merged using Samtools⁸⁵ v1.5. Peaks were called on the merged BAM using MACS2 (ref. 86) v2.2.1. Read counts per peak per sample were quantified using BEDTools⁸⁷ v2.26. Differential analysis for peaks was performed using DESeq2 1.30.1. Significant peaks are defined those as having an \log_2 fold change greater than 1 and an adjusted P value less than 0.05. Peaks were annotated by genomic feature using ChIP-seeker⁸⁸ v1.26.2 with UCSC mm9 genome annotation. Motif analyses for differentially enriched peaks were conducted using HOMER⁸⁹ v4.10.

CUT&RUN data processing and peak calling

Paired-end CUT&RUN reads were mapped to the UCSC mm9 mouse genome build (<https://genome.ucsc.edu>) using Bowtie v2.2.6. Read-alignment BAM files were processed with Picard Mark-Duplicates v2.17.0 (<https://broadinstitute.github.io/picard/>) to drop duplicate alignments and sorted by read-name using Samtools v1.5. Alignments were converted to BED format and subsequently to bedgraph format using BEDTools v2.29.2. Peaks were called with the SEACR⁹⁰ v1.3.

scRNA-seq library preparation, data processing and analysis

Tumours from five mice were pooled for each condition (control and SOX17-KO) and each timepoint (1, 2 and 4 weeks). To target a retention of 10,000 cells for each group, we counted and loaded ~16,000 sorted 7-AAD⁻EpCAM⁺CD45⁺ cells on the 10x Genomics assay as per the manufacturer's protocol, with 7.6% potential doublet rate according to 10x Genomics User Guide. To avoid the batch effect, all the 4-week samples were prepared on the same day, loaded on the same chip of the Chromium 10x, and sequenced in the same lane of a NextSeq 500 System (Illumina). All the 1-week and 2-week samples were prepared in the same manner. Data were processed using Cellranger version 6.0.1 with alignment to a modified version of the GENCODE mouse genome (GRCm38), version M23 (Ensembl 98) target provided by 10x genomics. Cellranger filtered data were imported into R version 4.1.0 (R Core Team 2021) and analysed with Seurat version 4.0.3 (ref. 91). In total, 5,560 cells (1-week control), 4,967 cells (2-week control), 6,952 cells (4-week control), 7,450 cells (1-week SOX17-KO), 3,145 cells (2-week SOX17-KO) and 6,429 cells (4-week SOX17-KO) were obtained. To exclude low-quality cells or empty droplets, cell doublets or multiplets, and low-quality or dying cells, cells with >500 and <5,500 detected genes, ≥200 unique molecular identifier (UMI) count per cell, and ≤10% mitochondrial transcripts were retained, resulting in 5,296 cells (96.2%: 1-week control), 4,585 cells (92.3%: 2-week control), 6,230 cells (89.6%: 4-week control), 7,047 cells (94.5%: 1-week SOX17-KO), 2,894 cells (92.0%: 2-week SOX17-KO) and 6,207 cells (96.5%: 4-week SOX17-KO) for further analysis. With an average of 93.5% cells retained, the doublet rate for our samples should be less than 6.5%. All the datasets were combined together using the merge function in Seurat. Data were normalized using NormalizeData function by a scale factor of 10,000, highly variable features were selected using FindVariableFeatures function with 2,000 features, and a linear transformation is performed using ScaleData function in Seurat. PCA was then performed on the scaled data using RunPCA function. We determined the dimensionality for further analysis based on the elbow plot drawn by ElbowPlot function and used 30 PCs to cluster the cells. UMAP was generated using the RunUMAP function with 30 principal components. For clustering of the cells, the FindNeighbors (with 30 PCs) and FindClusters functions in Seurat were used with the resolution

of 0.3. As each cluster contains cells from samples with different time-points and no sample-specific clusters are observed, we consider there is no obvious batch effect across our samples (Extended Data Figs. 6a and 7a). We also integrated these datasets using FindIntegrationAnchors and IntegrateData functions in Seurat to correct the possible batch effect, and confirmed analogous clustering pattern between the merged and integrated datasets, further demonstrating minimal batch effect. Thus, we used the merged datasets for downstream analysis. To define the cell type in each cluster, the data were queried for known immune cell-specific genes⁴³, and the specific expression of the marker genes in each cluster is confirmed by UMAP plots with gene expression using the FeaturePlot function in Seurat.

Statistical analysis

Unless otherwise specified in the figure legends or Methods, all experiments reported in this study were repeated at least three independent times. All sample number (n) of biological replicates and technical replicates, definition of centre, and dispersion and precision measures can be found in the figure legends. No statistical methods were used to predetermine sample size. The images for H&E staining, immunofluorescence and immunohistochemistry represent one of ≥6 biological replicates unless otherwise stated. Flow cytometry plots represent one of ≥3 biological replicates. All values are presented as mean ± s.d. unless otherwise stated. Intergroup comparisons were performed using unpaired two-tailed t -tests or one-way analysis of variance (ANOVA) with post-hoc Tukey's multiple comparison. For statistical assessment of differences in proportionality, Fisher's exact 2×2 test or chi-square test were performed. P values of <0.05 were considered to be significant. Statistical analysis was performed by GraphPad Prism. No sample or animals were excluded from analysis. Age- and sex-matched mice were randomly assigned to groups. Studies were not conducted blind with the exception of all histological analyses. Please note that statistical details are found in the figure legends.

Reporting summary

Further information on research design is available in the Nature Portfolio Reporting Summary linked to this article.

Data availability

Datasets generated in this study are available at the Gene Expression Omnibus (GEO) repository (GSE222713, token: ifylaumkx1svvqh): including RNA-seq data (GSE222709, GSE222710 and GSE245668), ATAC-seq data (GSE222712) and single-cell RNA-seq data (GSE222711). Any additional information required to reanalyse the data reported in this paper is available upon request.

49. Barker, N. et al. Identification of stem cells in small intestine and colon by marker gene *Lgr5*. *Nature* **449**, 1003–1007 (2007).
50. el Marjou, F. et al. Tissue-specific and inducible Cre-mediated recombination in the gut epithelium. *Genesis* **39**, 186–193 (2004).
51. Kuraguchi, M. et al. Adenomatous polyposis coli (APC) is required for normal development of skin and thymus. *PLoS Genet.* **2**, e146 (2006).
52. Johnson, L. et al. Somatic activation of the *K-ras* oncogene causes early onset lung cancer in mice. *Nature* **410**, 1111–1116 (2001).
53. Marino, S., Vooijis, M., van Der Gulden, H., Jonkers, J. & Berns, A. Induction of medulloblastomas in p53-null mutant mice by somatic inactivation of Rb in the external granular layer cells of the cerebellum. *Genes Dev.* **14**, 994–1004 (2000).
54. Hogquist, K. A. et al. T cell receptor antagonist peptides induce positive selection. *Cell* **76**, 17–27 (1994).
55. Chu, V. T. et al. Efficient generation of Rosa26 knock-in mice using CRISPR/Cas9 in C57BL/6 zygotes. *BMC Biotechnol.* **16**, 4 (2016).
56. Madisen, L. et al. A robust and high-throughput Cre reporting and characterization system for the whole mouse brain. *Nat. Neurosci.* **13**, 133–140 (2010).
57. Hao, Z. & Rajewsky, K. Homeostasis of peripheral B cells in the absence of B cell influx from the bone marrow. *J. Exp. Med.* **194**, 1151–1164 (2001).
58. Dow, L. E. et al. Apc restoration promotes cellular differentiation and reestablishes crypt homeostasis in colorectal cancer. *Cell* **161**, 1539–1552 (2015).
59. Boutin, A. T. et al. Oncogenic *Kras* drives invasion and maintains metastases in colorectal cancer. *Genes Dev.* **31**, 370–382 (2017).

Article

60. Fujii, M., Matano, M., Nanki, K. & Sato, T. Efficient genetic engineering of human intestinal organoids using electroporation. *Nat. Protoc.* **10**, 1474–1485 (2015).
61. Miyoshi, H. & Stappenbeck, T. S. In vitro expansion and genetic modification of gastrointestinal stem cells in spheroid culture. *Nat. Protoc.* **8**, 2471–2482 (2013).
62. Schwank, G. & Clevers, H. CRISPR/Cas9-mediated genome editing of mouse small intestinal organoids. *Methods Mol. Biol.* **1422**, 3–11 (2016).
63. Matano, M. et al. Modeling colorectal cancer using CRISPR-Cas9-mediated engineering of human intestinal organoids. *Nat. Med.* **21**, 256–262 (2015).
64. Drost, J. et al. Sequential cancer mutations in cultured human intestinal stem cells. *Nature* **521**, 43–47 (2015).
65. Koo, B. K. et al. Controlled gene expression in primary Lgr5 organoid cultures. *Nat. Methods* **9**, 81–83 (2011).
66. Pelosof, R. et al. Prediction of potent shRNAs with a sequential classification algorithm. *Nat. Biotechnol.* **35**, 350–353 (2017).
67. Dow, L. E. et al. A pipeline for the generation of shRNA transgenic mice. *Nat. Protoc.* **7**, 374–393 (2012).
68. Fellmann, C. et al. An optimized microRNA backbone for effective single-copy RNAi. *Cell Rep.* **5**, 1704–1713 (2013).
69. Mana, M. D. et al. High-fat diet-activated fatty acid oxidation mediates intestinal stemness and tumorigenicity. *Cell Rep.* **35**, 109212 (2021).
70. Cheng, C. W. et al. Ketone body signaling mediates intestinal stem cell homeostasis and adaptation to diet. *Cell* **178**, 1115–1131.e1115 (2019).
71. Beyaz, S. et al. High-fat diet enhances stemness and tumorigenicity of intestinal progenitors. *Nature* **531**, 53–58 (2016).
72. Sheridan, B. S. & Lefrancois, L. Isolation of mouse lymphocytes from small intestine tissues. *Curr. Protoc. Immunol.* **99**, 3.19.1–3.19.11 (2012).
73. Buenrostro, J. D., Wu, B., Chang, H. Y. & Greenleaf, W. J. ATAC-seq: a method for assaying chromatin accessibility genome-wide. *Curr. Protoc. Mol. Biol.* **109**, 21.29.21–21.29.29 (2015).
74. Skene, P. J., Henikoff, J. G. & Henikoff, S. Targeted *in situ* genome-wide profiling with high efficiency for low cell numbers. *Nat. Protoc.* **13**, 1006–1019 (2018).
75. Langmead, B., Trapnell, C., Pop, M. & Salzberg, S. L. Ultrafast and memory-efficient alignment of short DNA sequences to the human genome. *Genome Biol.* **10**, R25 (2009).
76. Li, B. & Dewey, C. N. RSEM: accurate transcript quantification from RNA-seq data with or without a reference genome. *BMC Bioinform.* **12**, 323 (2011).
77. Bullard, J. H., Purdom, E., Hansen, K. D. & Dudoit, S. Evaluation of statistical methods for normalization and differential expression in mRNA-seq experiments. *BMC Bioinform.* **11**, 94 (2010).
78. Patro, R., Duggal, G., Love, M. I., Irizarry, R. A. & Kingsford, C. Salmon provides fast and bias-aware quantification of transcript expression. *Nat. Methods* **14**, 417–419 (2017).
79. Soneson, C., Love, M. I. & Robinson, M. D. Differential analyses for RNA-seq: transcript-level estimates improve gene-level inferences. *F1000Res* **4**, 1521 (2015).
80. Love, M. I., Huber, W. & Anders, S. Moderated estimation of fold change and dispersion for RNA-seq data with DESeq2. *Genome Biol.* **15**, 550 (2014).
81. Zhu, A., Ibrahim, J. G. & Love, M. I. Heavy-tailed prior distributions for sequence count data: removing the noise and preserving large differences. *Bioinformatics* **35**, 2084–2092 (2019).
82. Mootha, V. K. et al. PGC-1 α -responsive genes involved in oxidative phosphorylation are coordinately downregulated in human diabetes. *Nat. Genet.* **34**, 267–273 (2003).
83. Han, T. et al. Lineage reversion drives WNT independence in intestinal cancer. *Cancer Discov.* **10**, 1590–1609 (2020).
84. Subramanian, A. et al. Gene set enrichment analysis: a knowledge-based approach for interpreting genome-wide expression profiles. *Proc. Natl Acad. Sci. USA* **102**, 15545–15550 (2005).
85. Li, H. et al. The Sequence Alignment/Map format and SAMtools. *Bioinformatics* **25**, 2078–2079 (2009).
86. Feng, J., Liu, T., Qin, B., Zhang, Y. & Liu, X. S. Identifying ChIP-seq enrichment using MACS. *Nat. Protoc.* **7**, 1728–1740 (2012).
87. Quinlan, A. R. & Hall, I. M. BEDTools: a flexible suite of utilities for comparing genomic features. *Bioinformatics* **26**, 841–842 (2010).
88. Wang, Q. et al. Exploring epigenomic datasets by ChIPseeker. *Curr. Protoc.* **2**, e585 (2022).
89. Heinz, S. et al. Simple combinations of lineage-determining transcription factors prime cis-regulatory elements required for macrophage and B cell identities. *Mol. Cell* **38**, 576–589 (2010).
90. Meers, M. P., Tenenbaum, D. & Henikoff, S. Peak calling by sparse enrichment analysis for CUT&RUN chromatin profiling. *Epigenetics Chromatin* **12**, 42 (2019).
91. Hao, Y. et al. Integrated analysis of multimodal single-cell data. *Cell* **184**, 3573–3587.e3529 (2021).

Acknowledgements The authors thank the Swanson Biotechnology Center at the Koch Institute, which encompasses the Flow Cytometry, Histology, Microscopy and Genomics and Bioinformatics Core facilities (NCI P30-CA14051); the Department of Comparative Medicine for mouse husbandry support; S. Holder and members of the Hope Babette Tang (1983) Histology Facility for substantial histology support; members of the Yilmaz laboratory for discussions; K. Kelley for laboratory management; L. Galoyan for administrative assistance; K. W. Wucherpfennig for reading of the manuscript; L. M. LaFave for help and advice with the ATAC-seq experiments; C. P. Concepcion for help and advice with the CUT&RUN experiments; and A. Bhutkar for help and advice for the RNA-seq and ATAC-seq analyses. N.G. is supported by Postdoctoral Fellowship for Research Abroad from Japan Society for the Promotion of Science and 1K99AG076987-01A1. S.G. is supported by the research grant of Astellas Foundation and Postdoctoral Fellowship for Research Abroad from Japan Society for the Promotion of Science. Ö.H.Y. is supported by R01CA254314, R01CA257523, R01DK126545, R01DK133919, and U54CA224068; a Pew-Stewart Trust scholar award; AFAR and Glenn Foundation for Medical Research Breakthroughs in Gerontology (BIG) Award; Kenneth Rainin Foundation Innovator Award; and a Crohn's & Colitis Foundation Senior Research Award. Ö.H.Y. receives support from the MIT Stem Cell Initiative via Foundation MIT. J.A. is supported by R01DK132544, the Smith Family Awards Program for Excellence in Biomedical Research, the Ludwig Center at Harvard, the Ira Schneider Foundation, the Claudia Adams Barr Program in Innovative Basic Cancer Research Program, and the Innovation Research Funds at DFCI. J.A. is a member of the Parker Institute for Cancer Immunotherapy and a New York Stem Cell Foundation-Robertson Investigator, and her research is funded, in part, by these two institutes. Ö.H.Y. and J.A. together are supported by the Footbridge and Traditional Bridge Koch Institute-Dana-Farber Cancer Institute awards.

Author contributions N.G., P.M.K.W., T.J., J.A. and Ö.H.Y. conceived the study. N.G., P.M.K.W., S.G., J.A. and Ö.H.Y. designed the experiments. N.G. performed most of the experiments. P.M.K.W. assisted with co-culture experiments of T cells and organoids and provided reagents. S.G. performed the autochthonous mouse adenoma model experiments. P.M.K.W. assisted with the RNA-seq and ATAC-seq analyses. S.I. and S.G. assisted organoid orthotopic transplantation experiments. J.B. generated mouse naive AKP organoids. G.E. established healthy human colon organoids from patients. M.S.T. and V.D. provided human histopathological samples with diagnostic information and assisted in the interpretation of histology. N.G., J.A., and Ö.H.Y. wrote the paper. All the authors assisted in the interpretation of the experiments and the editing of the paper.

Competing interests Ö.H.Y. holds equity and is a scientific advisory board member in Ava Lifesciences and AI Proteins. Ö.H.Y. receives research support from Microbial Machines. Ö.H.Y. is a consultant for Nestle. T.J. is a member of the Board of Directors of Amgen and Thermo Fisher Scientific and a co-founder of Dragonfly Therapeutics and T2 Biosystems; serves on the Scientific Advisory Board of Dragonfly Therapeutics, SQZ Biotech, and Skyhawk Therapeutics; and is president of Break Through Cancer. The laboratory of T.J. currently receives funding from Johnson & Johnson and The Lustgarten Foundation, but these funds did not support the research described in this manuscript. The other authors declare no competing interests.

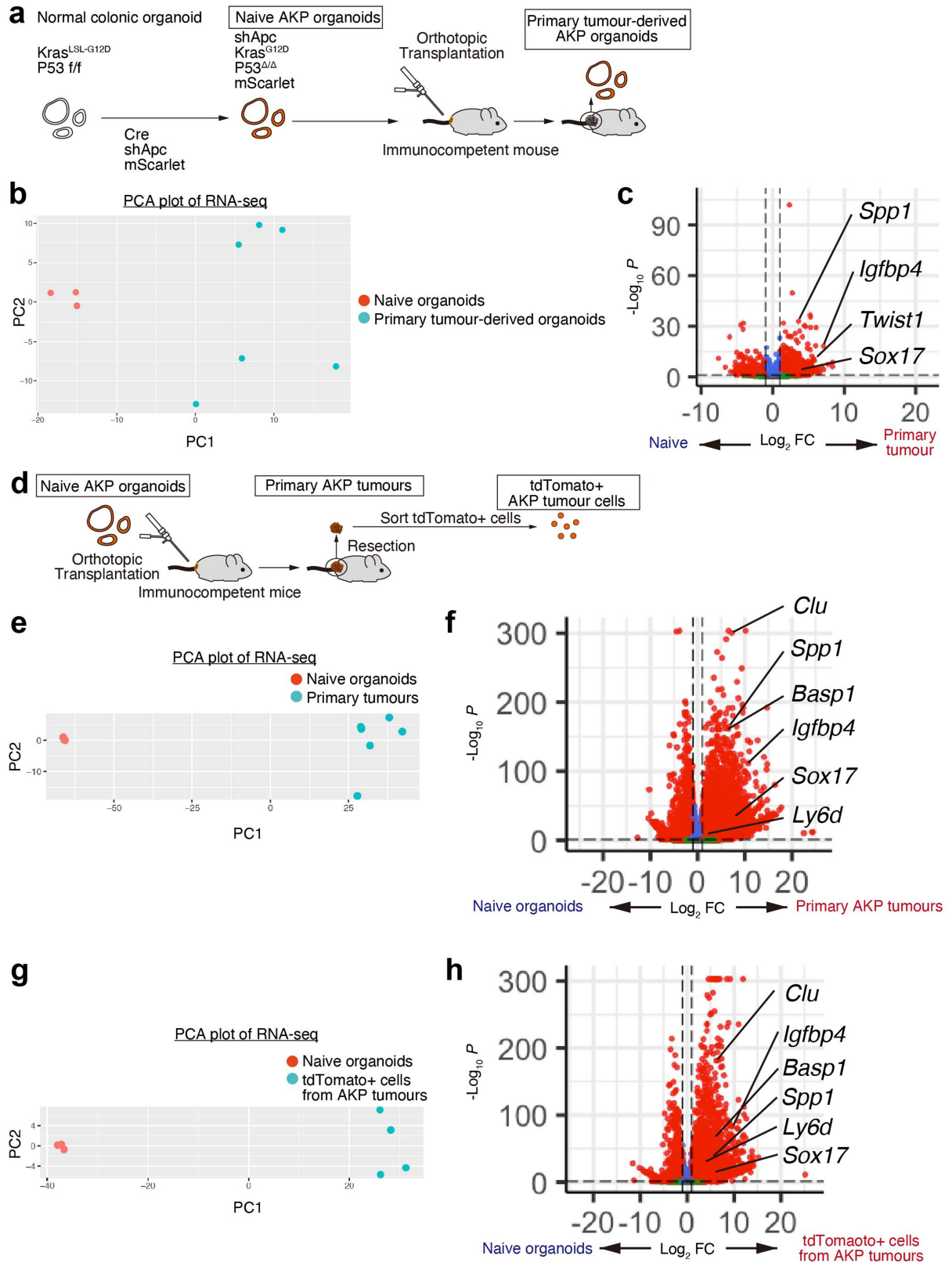
Additional information

Supplementary information The online version contains supplementary material available at <https://doi.org/10.1038/s41586-024-07135-3>.

Correspondence and requests for materials should be addressed to Judith Agudo or Ömer H. Yilmaz.

Peer review information *Nature* thanks Ophir Klein, Sean Morrison and the other, anonymous, reviewer(s) for their contribution to the peer review of this work.

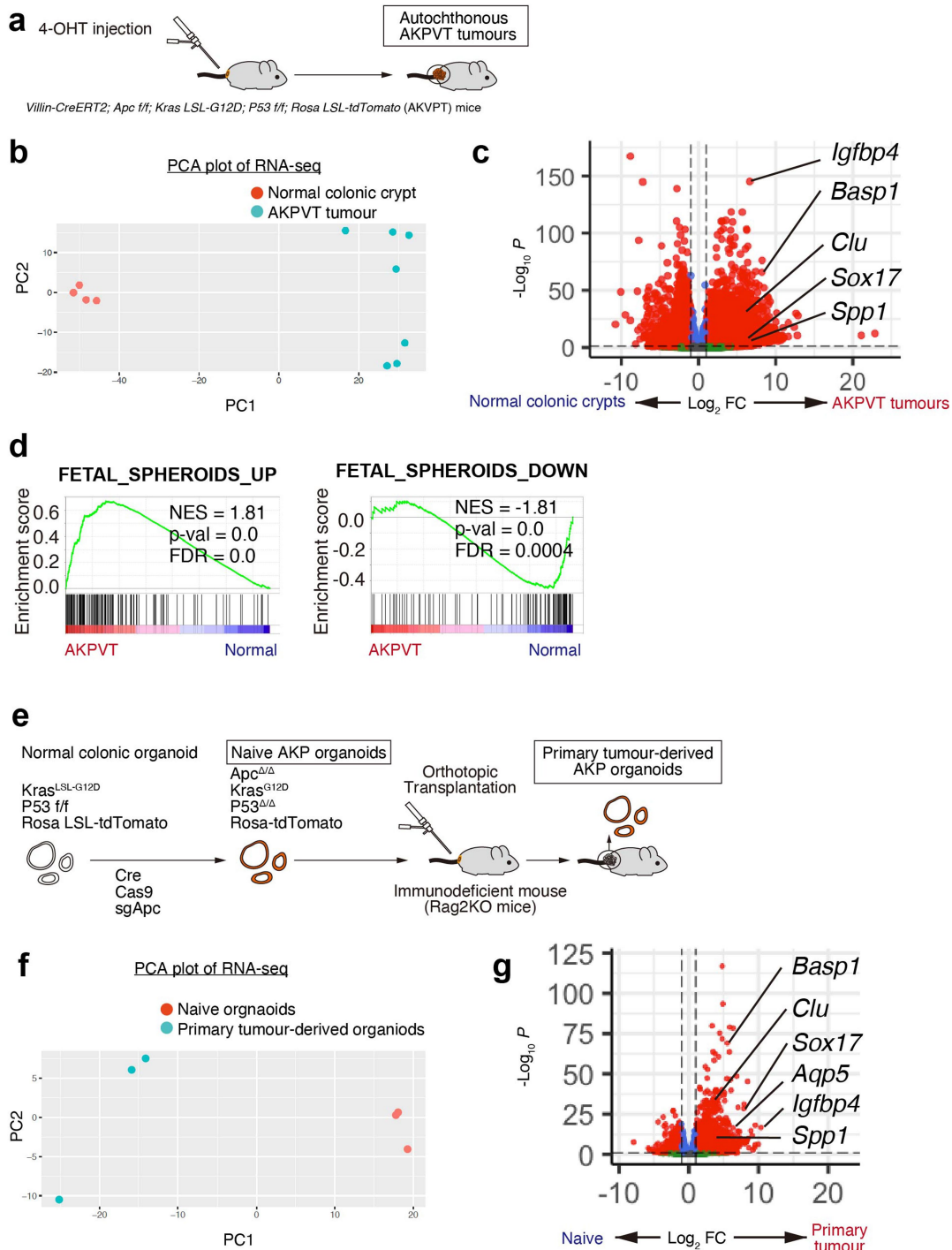
Reprints and permissions information is available at <http://www.nature.com/reprints>.



Extended Data Fig. 1 | In vivo transplantation of naïve AKP organoids induces SOX17 expression. **a**, Schematic of generation of mouse naïve AKP organoids by shApc and primary tumour-derived AKP organoids from immunocompetent mice by colonoscopy-based orthotopic transplantation. **b, c**, PCA plot (**b**) and volcano plot (**c**) of RNA-seq in naïve and primary tumour-derived AKP organoids (shApc model) from immunocompetent mice. $n = 3\text{--}6$ mice per group. **d**, Schematic of RNA-seq in bulk resected primary tumours as well as in

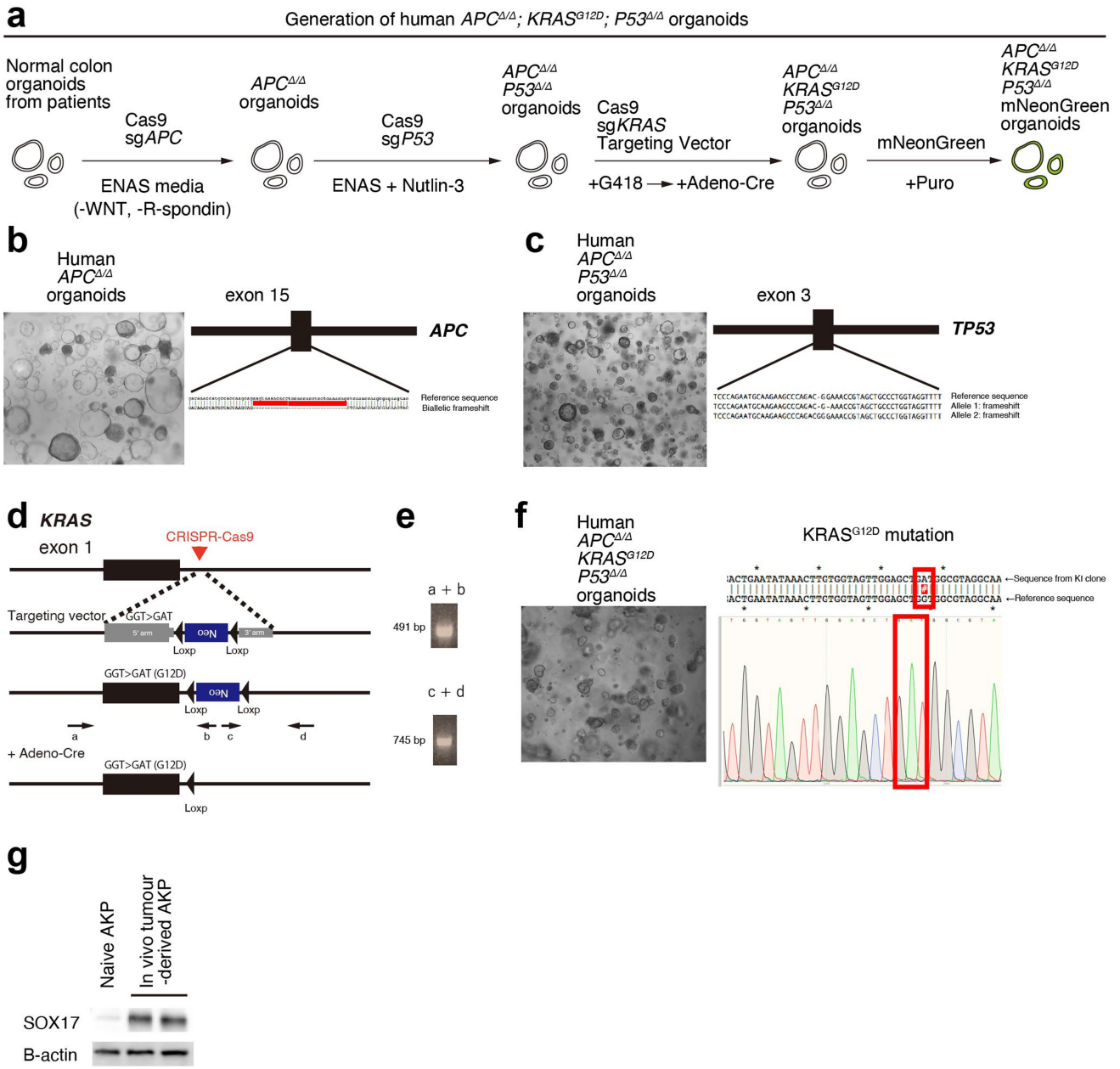
flow cytometry-sorted tdTomato+ tumour cells that were freshly isolated from primary tumours. **e, f**, PCA plot (**e**) and volcano plot (**f**) of RNA-seq in naïve AKP organoids and bulk resected primary tumours. $n = 3\text{--}6$ mice per group. **g, h**, PCA plot (**g**) and volcano plot (**h**) of RNA-seq in naïve AKP organoids and flow cytometry-sorted tdTomato+ tumour cells that were freshly isolated from primary tumours. $n = 3\text{--}4$ mice per group.

Article



Extended Data Fig. 2 | Autochthonous tumours and transplanted tumours in immunodeficient mice show elevated SOX17 expression. **a**, Autochthonous tumour models by colonoscopy-guided 4-OH-Tamoxifen injection into the colonic mucosa of *Villin-CreERT2; Apc f/f; Kras LSL-G12D; P53 f/f; Rosa LSL-tdTomato* (AKPVT) mice. **b-d**, PCA plot (**b**), volcano plot (**c**), and GSEA (**d**) of RNA-seq in normal colon and autochthonous AKPVT tumours. n = 4–7 mice per group.

e, Schematic of generation of mouse naïve AKP organoids and mouse primary tumour-derived AKP organoids from immunodeficient mice (*Rag2*^{−/−} mice) by colonoscopy-based orthotopic transplantation. **f,g**, PCA plot (**f**) and volcano plot (**g**) of RNA-seq in naïve and primary tumour-derived AKP organoids from immunodeficient mice. n = 3 mice per group.

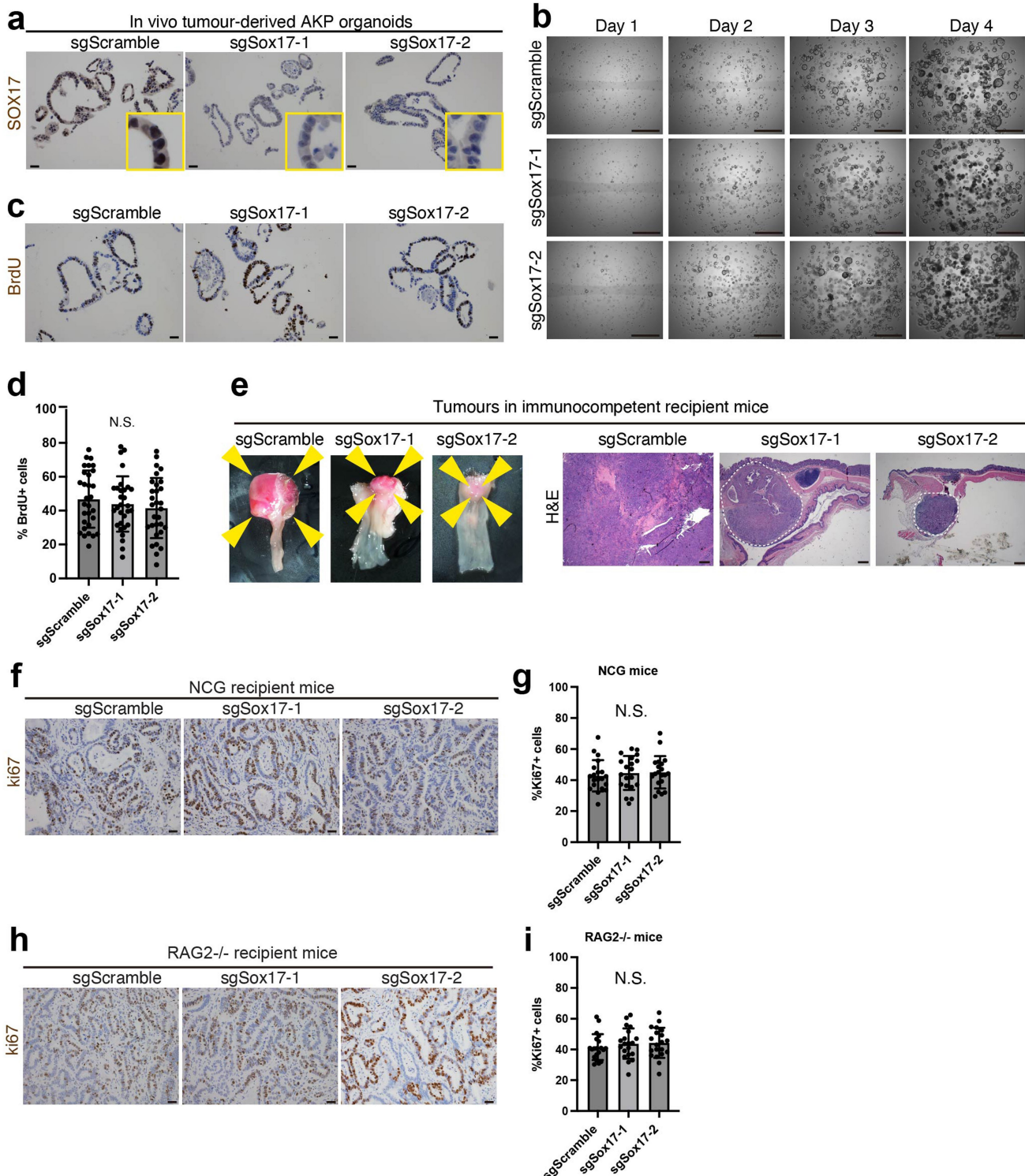


Extended Data Fig. 3 | Generation of human naive AKP organoids.

a, Schematic of generation of human naive AKP organoids by CRISPR-Cas9 editing. **b**, Representative image of human $APC^{\Delta/\Delta}$ organoids and Sanger sequencing result confirming the biallelic frameshift mutations in APC . **c**, Representative image of human $APC^{\Delta/\Delta}$; $P53^{\Delta/\Delta}$ organoids and Sanger sequencing result confirming the biallelic frameshift mutations in $TP53$.

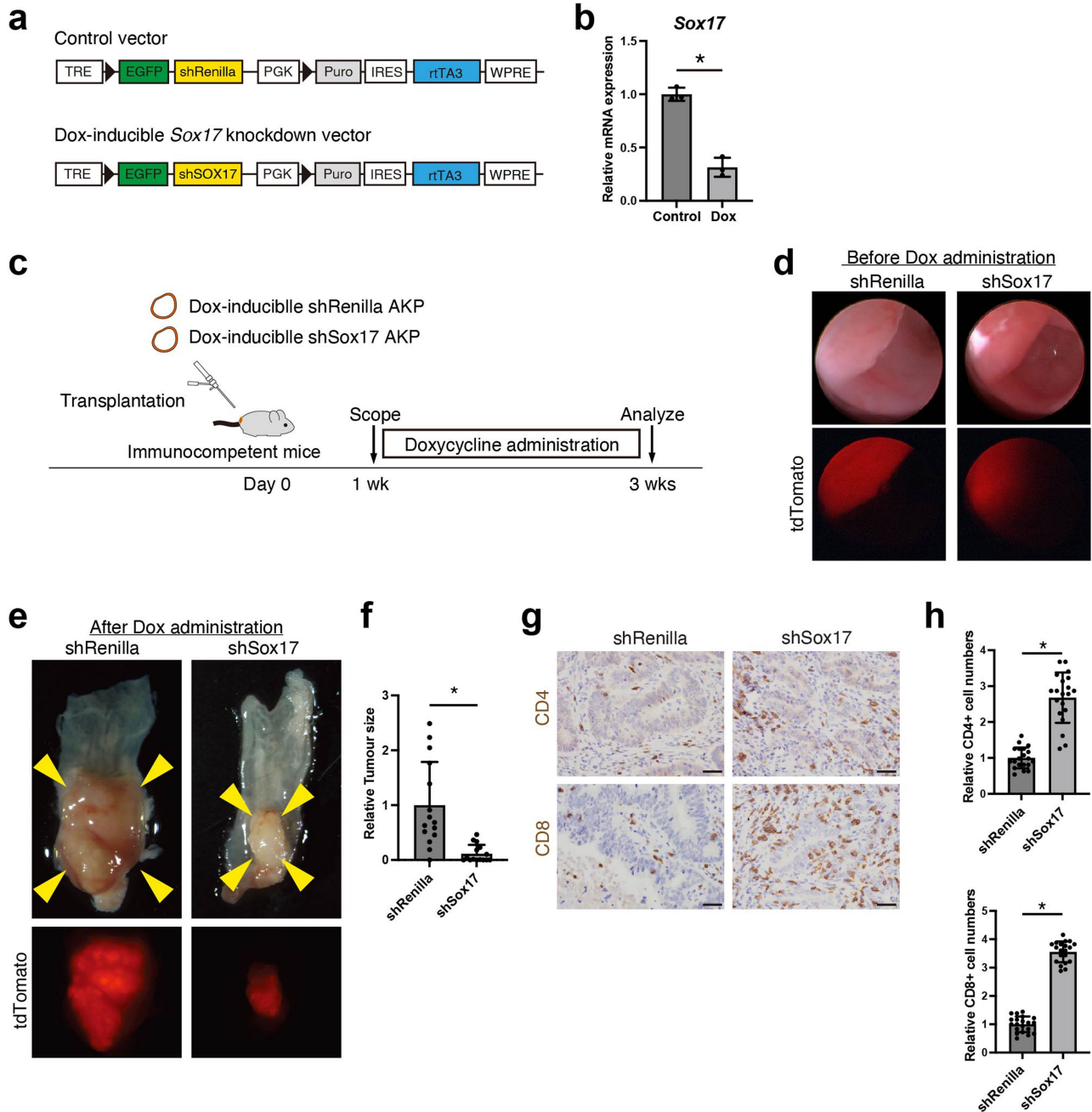
d, e, Strategy to knock in a $KRAS^{G12D}$ point mutation by homology directed repair (**d**), and PCR results confirming the correct homology directed repair (**e**). **f**, Representative image of human $APC^{\Delta/\Delta}$; $KRAS^{G12D}$; $P53^{\Delta/\Delta}$ organoids and the Sanger sequencing result confirming the $KRAS^{G12D}$ point mutation. **g**, Immunoblots for SOX17 in human naive AKP organoids and in vivo tumour-derived human AKP organoids.

Article



Extended Data Fig. 4 | SOX17 loss does not affect tumour growth/proliferation in immunodeficient mice. **a**, IHC for SOX17 in sgScramble, sgSox17-1, and sgSox17-2 in vivo tumour-derived AKP organoids. **b**, Time-course images of sgScramble, sgSox17-1, and sgSox17-2 AKP organoids. 2,000 single cells in 10 μ l Matrigel were plated for each well. Representative of 10 wells. Representative of three independent experiments. See also Fig. 2c for organoid growth curve. **c, d**, IHC for BrdU (**c**) and the percentage of BrdU+ cells (**d**) in sgScramble, sgSox17-1, and sgSox17-2 AKP organoids that were incubated for 4 hrs with 10 μ M BrdU in the culture media. n = 30 organoids per group. **e**, Representative images and

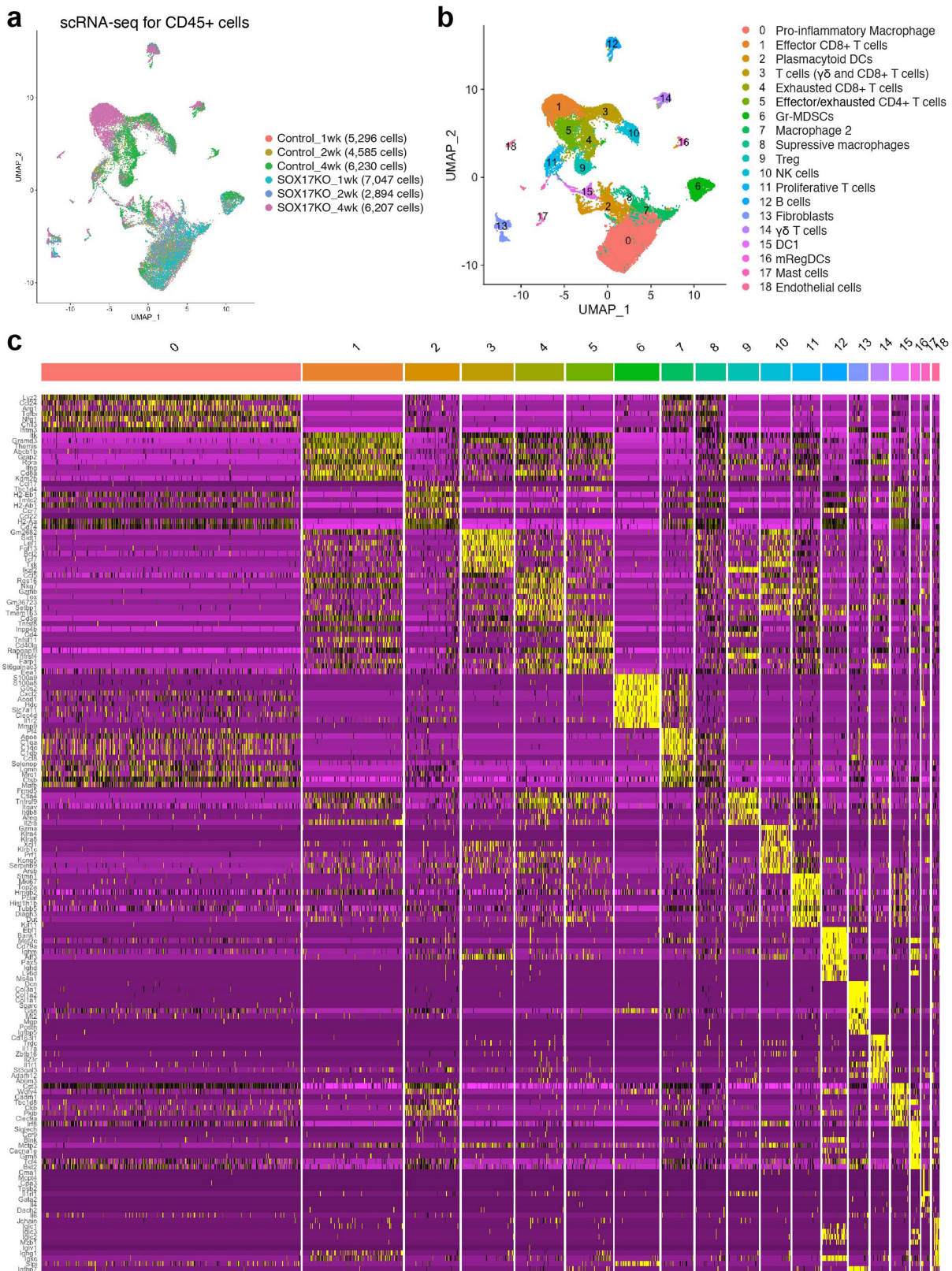
H&E staining of orthotopically transplanted sgScramble, sgSox17-1, and sgSox17-2 AKP tumours in immunocompetent mice. **f, g**, IHC for Ki67 (**f**) and quantification (**g**) in orthotopically transplanted sgScramble, sgSox17-1, and sgSox17-2 AKP tumours in NCG mice. n = 20 fields from 5 mice per group. **h, i**, IHC for Ki67 (**h**) and quantification (**i**) in orthotopically transplanted sgScramble, sgSox17-1, and sgSox17-2 AKP tumours in *Rag2^{-/-}* mice. n = 20 fields from 5 mice per group. One-way ANOVA (**d, g, i**). Data are mean \pm SD. N.S. not significant. Scale bar, 20 μ m (**a, c, f, h**), 1000 μ m (**b**), 500 μ m (**e**).



Extended Data Fig. 5 | *Sox17* knockdown in established AKP tumours inhibits tumour growth. **a**, Constructs for *Sox17* knockdown and control. **b**, qRT-PCR for *Sox17* mRNA expression 48 hr after doxycycline administration. $n = 3$ organoid culture wells per group. **c**, Schematic of *Sox17* knockdown in established AKP tumours using doxycycline-inducible system. **d**, Tumour formation was confirmed by colonoscopy 1 week after the transplantation. **e**, **f**, Representative

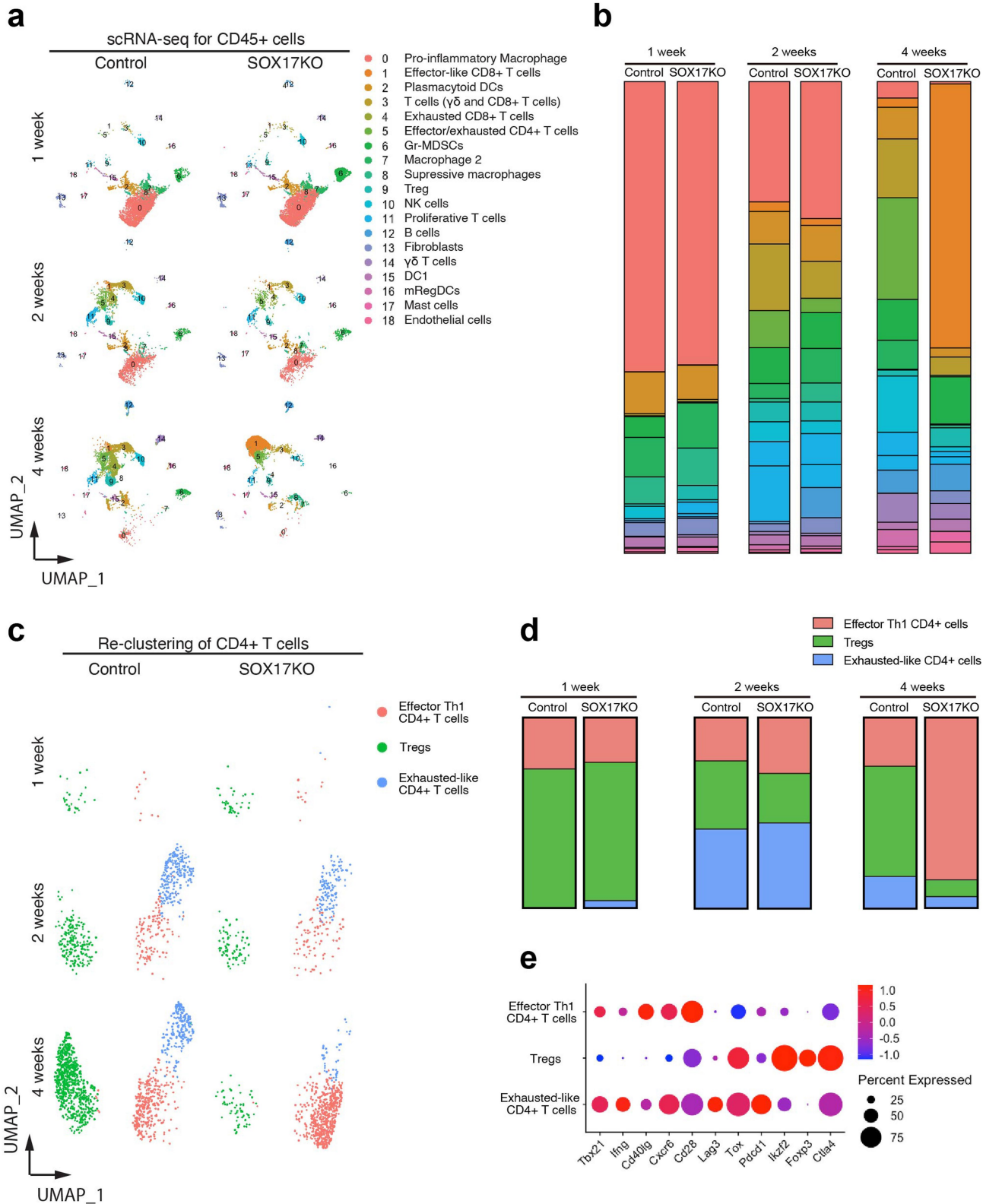
images (e) and tumour size (f) 2 weeks after doxycycline administration. $n = 15$ mice per group. Pooled from three independent experiments. **g**, **h**, IHC for CD4 and CD8 (g) and quantification (h) in control (shRenilla) and *Sox17* knockdown (sh*Sox17*) tumours. $n = 20$ fields from 5 mice per group. Unpaired two-tailed t-tests (b, f, h). Data are mean \pm SD. * $p < 0.05$. Scale bar, 20 μ m (g).

Article



Extended Data Fig. 6 | Time-course analysis of scRNA-seq of immune cells in control and SOX17-null tumours. **a, b**, UMAP plots of CD45+ cells in control and SOX17KO AKP tumours at 1-, 2- and 4-weeks post-transplantation. Classified by sample groups (**a**) and cell clusters (**b**). Control at 1 wk; n = 5,296 cells, control at 2 wks; n = 4,585 cells; control at 4 wks; n = 6,230 cells, SOX17KO

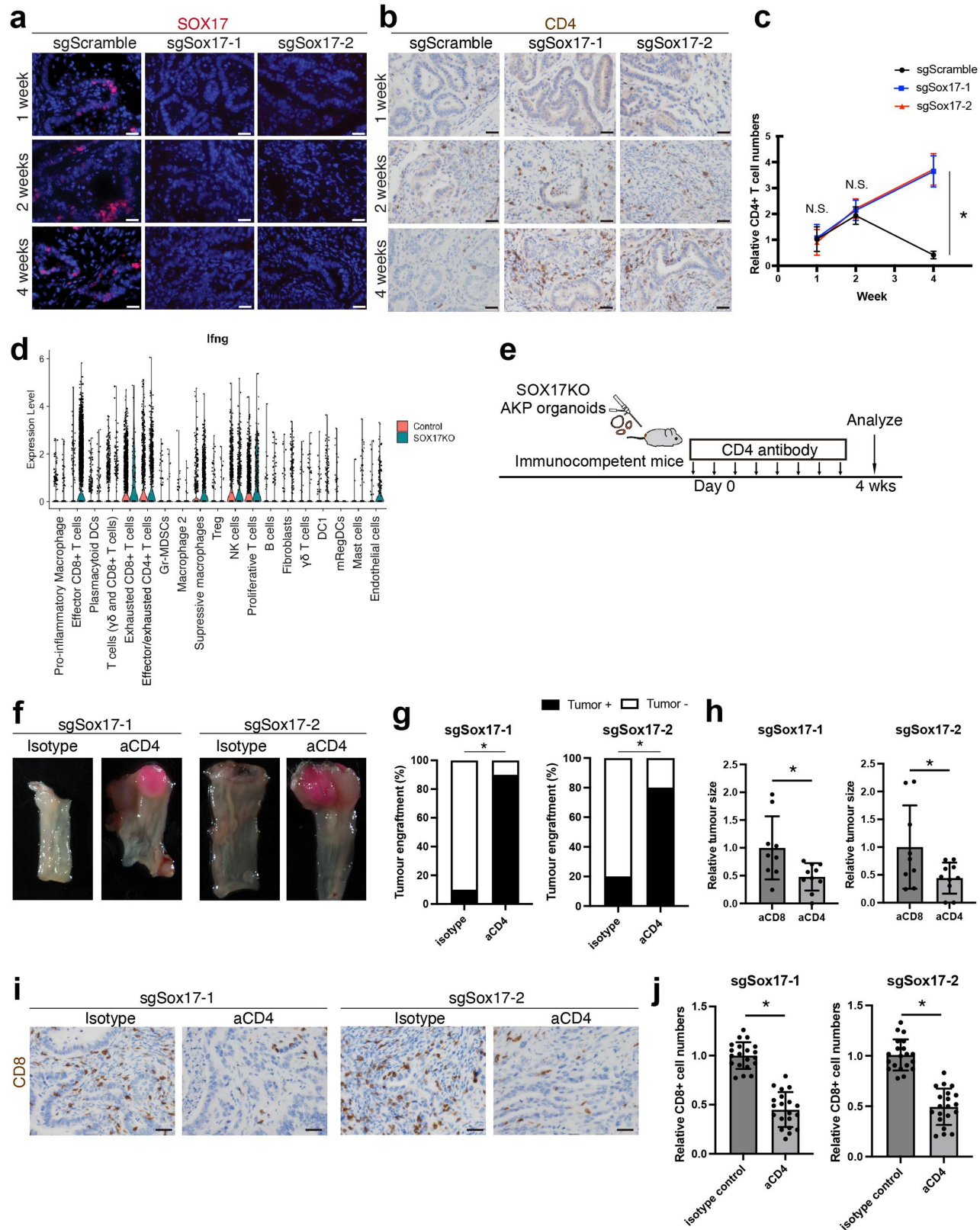
at 1 wk; n = 7,047 cells, SOX17KO at 2 wks; n = 2,894 cells, SOX17KO at 4 wks; n = 6,207 cells, pooled from 5 mice in each group. **c**, Expressions of key genes used for identification of major populations in the scRNA-seq analysis of control and SOX17KO tumours.



Extended Data Fig. 7 | SOX17 alters CD4⁺ T cell subsets in AKP CRCs. **a, b**, Time-course analysis of CD45⁺ cells in control and SOX17KO AKP tumours at 1-, 2- and 4-weeks post-transplantation by scRNA-seq. UMAP plots (a). Bar graphs showing %

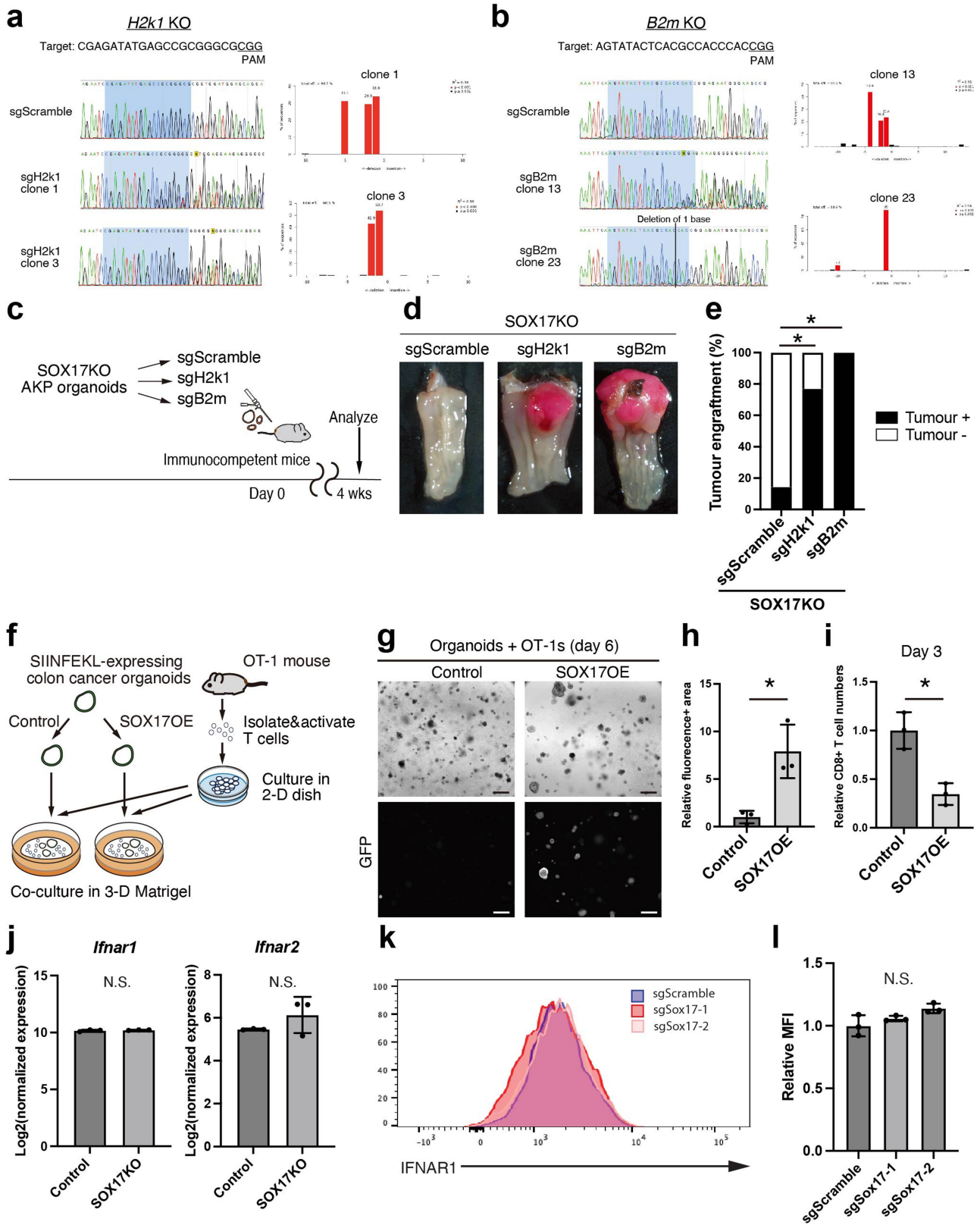
of each subcluster (b). **c-e**, UMAP plots (c) of re-clustering of CD4⁺ T cell clusters (clusters 5 and 9 in Extended Data Fig. 7b). Bar graphs showing % of each subcluster (d). Dot plots of gene expressions in each subcluster (e).

Article



Extended Data Fig. 8 | Effector Th1 CD4⁺ T cells contribute to the elimination of SOX17-null tumours. **a-c**, IHC for SOX17 (**a**) and CD4 (**b**) and quantification (**c**) in sgScramble, sgSox17-1, and sgSox17-2 AKP tumours at 1-, 2- and 4-weeks post-transplantation. n = 20 fields from 5 mice per group. **d**, Violin plot for *Ifng* expression in scRNA-seq data from Extended Data Fig. 6a. **e-g**, Schematic (**e**), representative images (**f**), and tumour engraftment rate (**g**) of orthotopically transplanted SOX17KO (sgSox17-1 and sgSox17-2) AKP tumours in isotype control- and anti-CD4 antibody-treated mice. n = 10 mice per group.

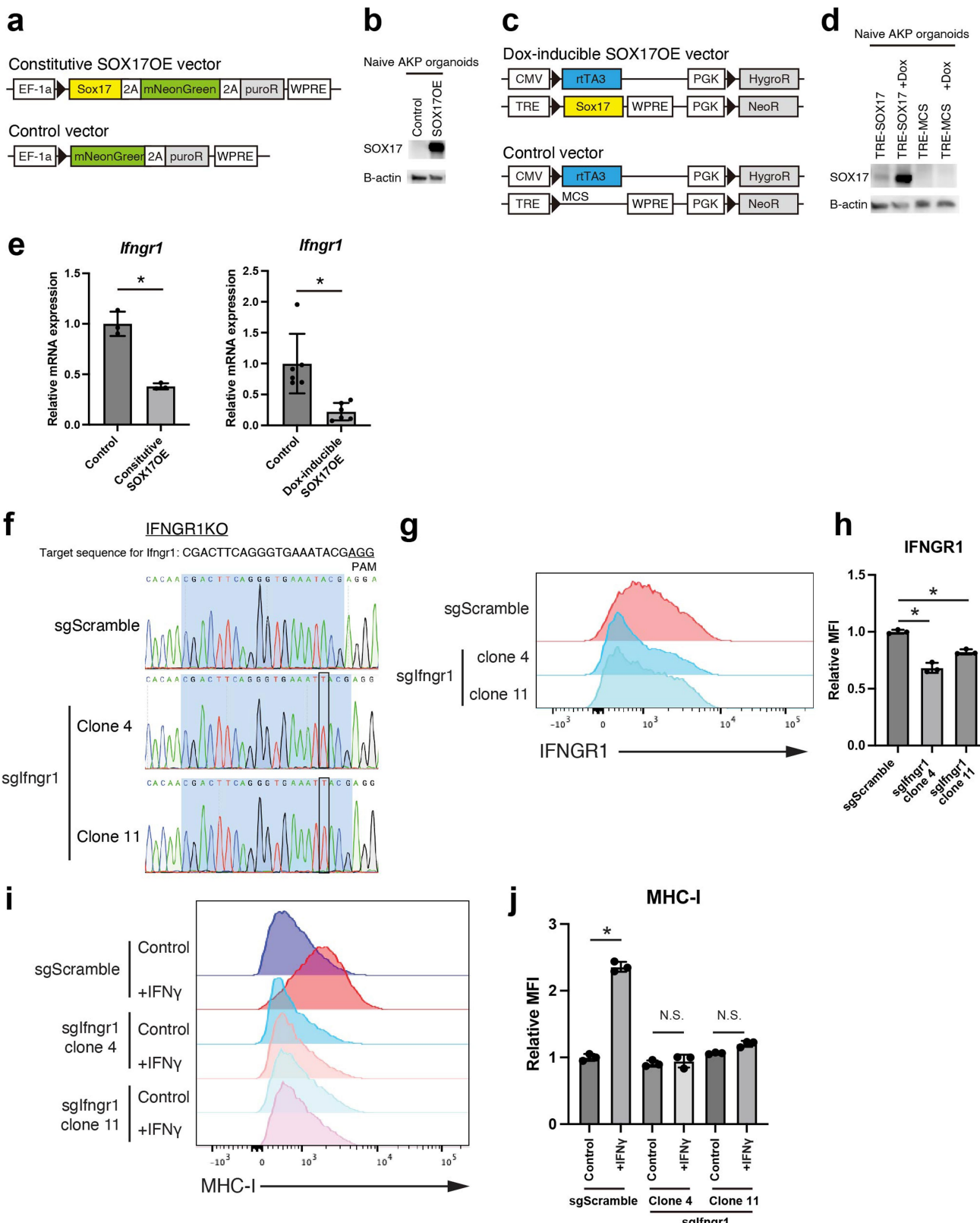
Pooled from two independent experiments. **h**, SOX17-null tumour size in anti-CD4 antibody and anti-CD8 antibody-treated mice. n = 9–10 mice per group. Pooled from two independent experiments. **i,j**, IHC for CD8 (**i**) and quantification (**j**) in isotype control- and anti-CD4 antibody-treated mice. n = 20 fields from 5 mice. One-way ANOVA (**g**). Fisher's exact test (**g**). Unpaired two-tailed t-tests (**h,j**). Data are mean ± SD. *p < 0.05. Scale bar, 25 μm (**a**), 20 μm (**b,i**).



Extended Data Fig. 9 | SOX17 expression augments the resistance of colon cancer cells to CD8+ T cell-mediated killing. **a-b**, Sanger sequencing chromatograms and TIDE analyses for sgH2k1 clones (**a**) and sgB2m clones (**b**). **c-e**, Schematic (**c**), representative images (**d**), and tumour engraftment rate (**e**) of orthotopic transplantation of SOX17KO (sgSox17-1); sgScramble, SOX17KO; H2K1KO (sgH2k1 clone 3), and SOX17KO; B2M KO (sgB2m clone 23) AKP organoids into the colons of immunocompetent mice. $n = 7\text{-}13$ mice per group. **f**, Schematic of co-culture experiments of SOX17OE SIINFEKL-expressing colon

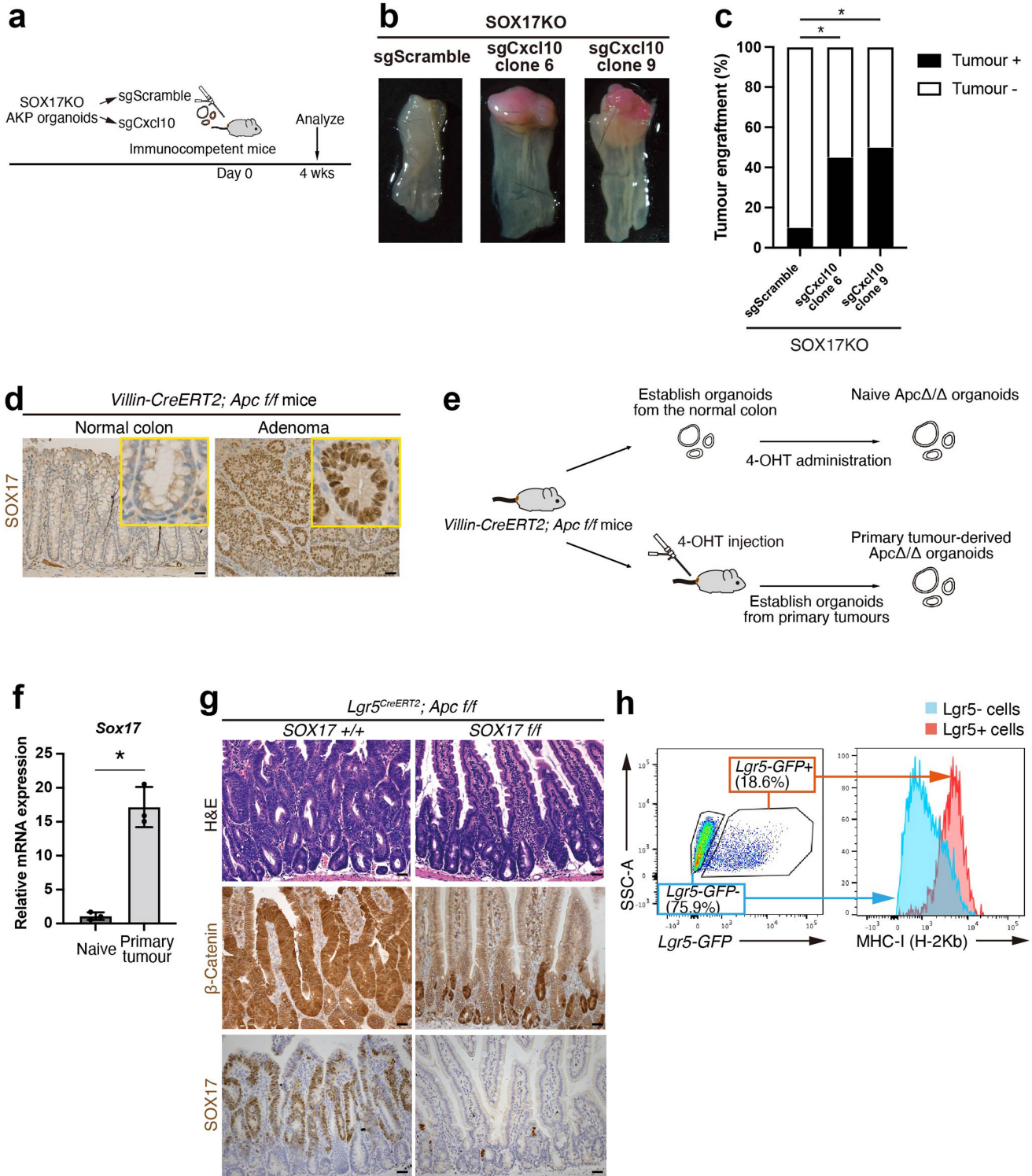
cancer organoids with activated OT-1T cells. **g-i**, Representative images (**g**), and quantification of organoids (**h**) and CD8+ T cell numbers (**i**) in the co-culture experiments. $n = 3$ per group. **j**, *Ifnar1* and *Ifnar2* expression by RNA-seq data of control and SOX17KO AKP organoids. $n = 3$ per group. **k-l**, Flow cytometry analysis of protein surface levels of IFNAR1 (**k**) and quantification (**l**). $n = 3$ per group. Chi-square test (**e**). Unpaired two-tailed t-tests (**h, i**). One-way ANOVA (**l**). Data are mean \pm SD. * $p < 0.05$. N.S. not significant. Scale bar, 500 μm (**h**).

Article



Extended Data Fig. 10 | Generation of SOX17 overexpression organoids and IFNGR1 knockout organoids. **a**, Constructs for constitutive SOX17 overexpression (SOX17OE). **b**, Immunoblots confirmed SOX17 overexpression in naïve AKP organoids transduced with a constitutive SOX17OE cassette. **c**, Constructs for dox-inducible SOX17OE. **d**, Immunoblots confirmed SOX17 overexpression in naïve AKP organoids transduced with a dox-inducible SOX17OE cassette 72 h after doxycycline administration. **e**, qRT-PCR for *Ifngr1* mRNA

expression in constitutive and dox-inducible SOX17OE AKP organoids compared with controls. $n = 3-6$ each group. **f**, Sanger sequencing chromatograms for IFNGR1KO clones. **g**, **h**, Flow cytometry (**g**) and quantification (**h**) of IFNGR1 expression. $n = 3$ per group. **i**, **j**, Flow cytometry (**i**) and quantification (**j**) of MHC-I expression 24 h after IFN γ (10 ng/ml) administration in the organoids. $n = 3$ per group. One-way ANOVA (**h**). Unpaired two-tailed t-test (**j**). Data are mean \pm SD. N.S. not significant.



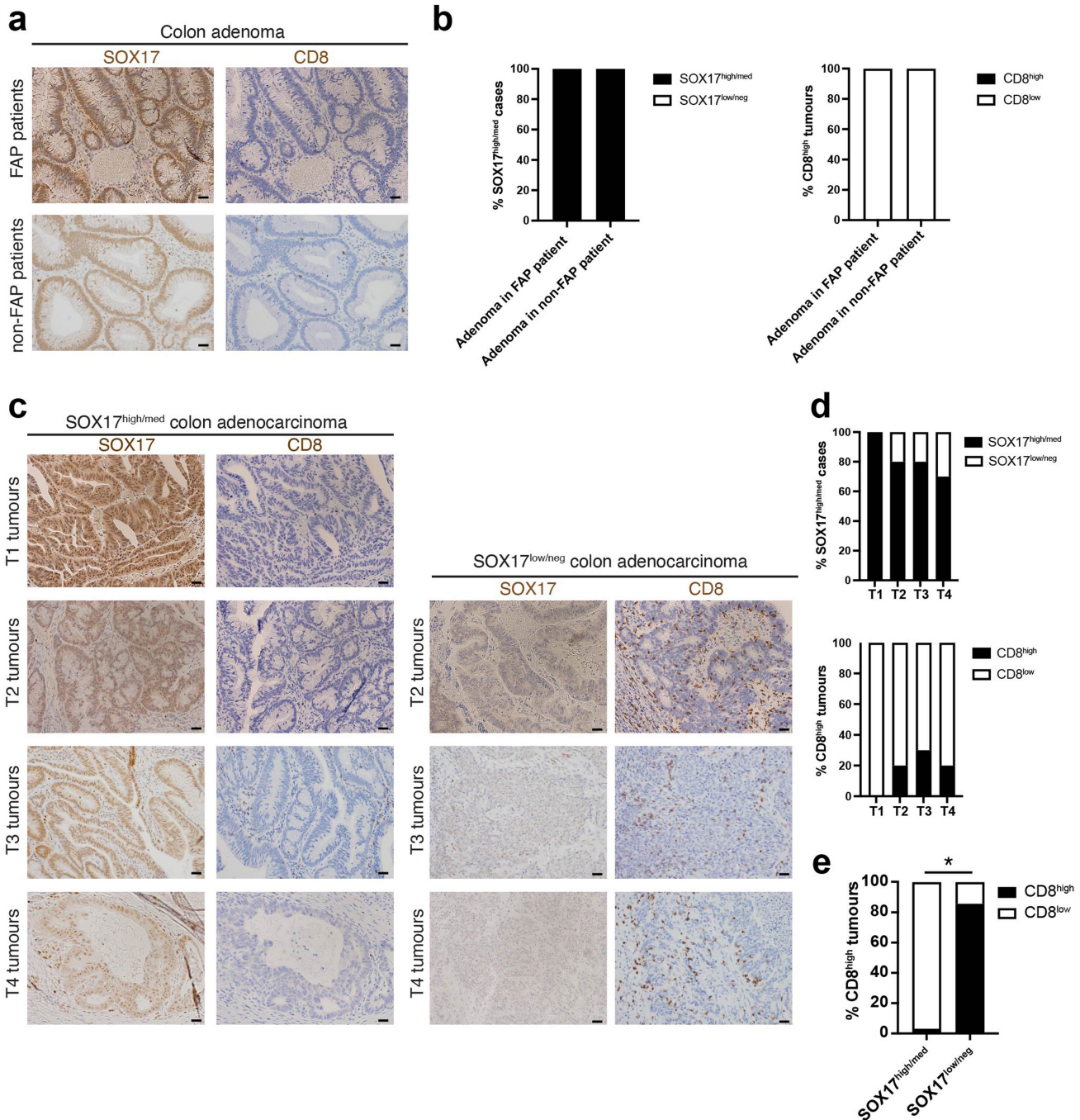
Extended Data Fig. 11 | In vivo APC loss induces SOX17 expression.

a-c, Schematic (a), representative images (b), and tumour engraftment rate (c) of orthotopic transplantation of SOX17KO (sgSox17-1) and SOX17KO; CXCL10KO (sgCxcl10 clones 6 and 9) AKP organoids into immunocompetent recipient mice. n = 20 mice per group. Sanger sequencing results of CXCL10KO organoids are in Supplementary Fig. 4. **d**, IHC for SOX17 in *Villin-CreERT2; Apc f/f* mouse normal colon and adenoma. **e**, Schematic of generation of naïve and primary tumour-derived *Apc*^{-/-} organoids. **f**, qRT-PCR for *Sox17*mRNA expression in

naïve and primary tumour-derived *Apc*^{-/-} organoids. n = 3 mice per group.

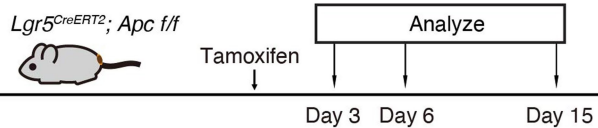
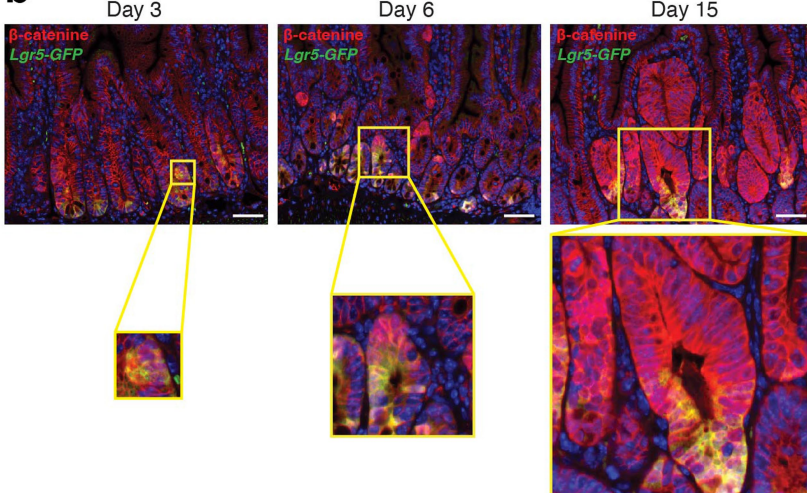
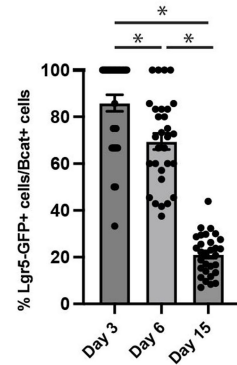
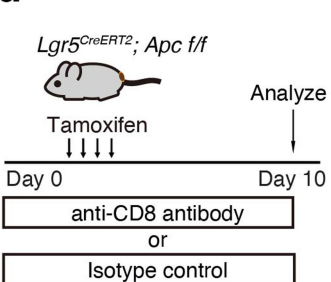
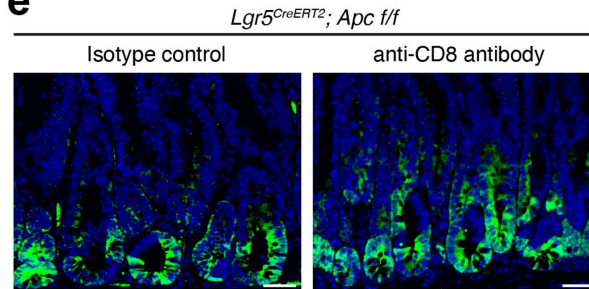
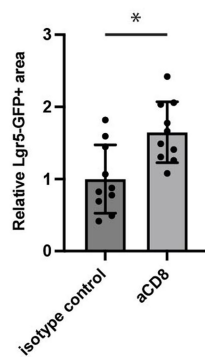
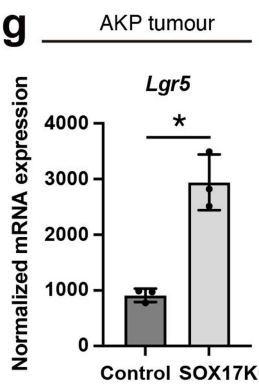
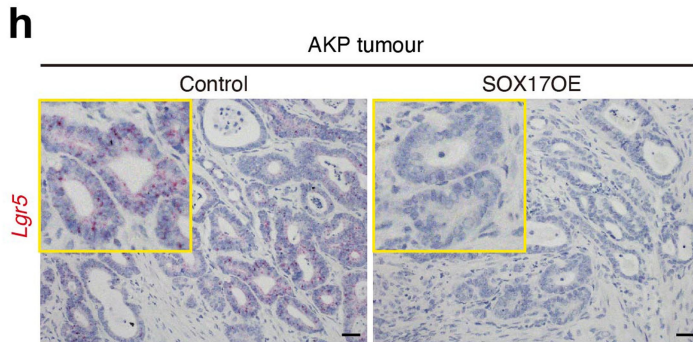
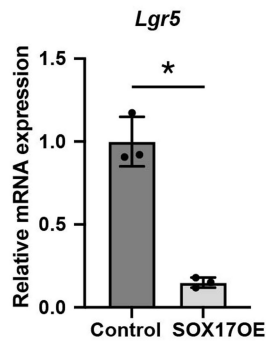
g, H&E staining and IHC for β-Catenin and SOX17 in *Lgr5-CreERT2; Apc f/f* and *Lgr5-CreERT2; Apc f/f; Sox17 f/f* mouse intestines after tamoxifen injections. Representative of n = 6 mice per group. **h**, Flow cytometry of MHC-I (H-2Kb) expression in *Lgr5-GFP+* and *Lgr5-GFP-* cells from *Lgr5-CreERT2; Apc*^{-/-} adenoma. n = 4 mice. See Fig. 5i for quantification. Chi-square test (c). Unpaired two-tailed t-test (f). Data are mean ± SD. *p < 0.05. Scale bar, 20 μm (d,g).

Article



Extended Data Fig. 12 | SOX17 expression in human adenomas and CRCs anti-correlates with CD8+ T cell infiltration. **a, b,** Representative images (a) and classification (b) of IHC for SOX17 and CD8 in adenomas from patients with (n = 8) or without (n = 11) familial adenomatous polyposis (FAP). **c–e,** Representative images (c) and classification (d) of IHC for SOX17 and CD8 in CRC samples at different pathologic tumour stages (pT1: n = 9, pT2: n = 10, pT3: n = 10, pT4: n = 10). Plot (e) showing the % of CD8^{high} tumours and CD8^{low} tumours in SOX17^{high/med}

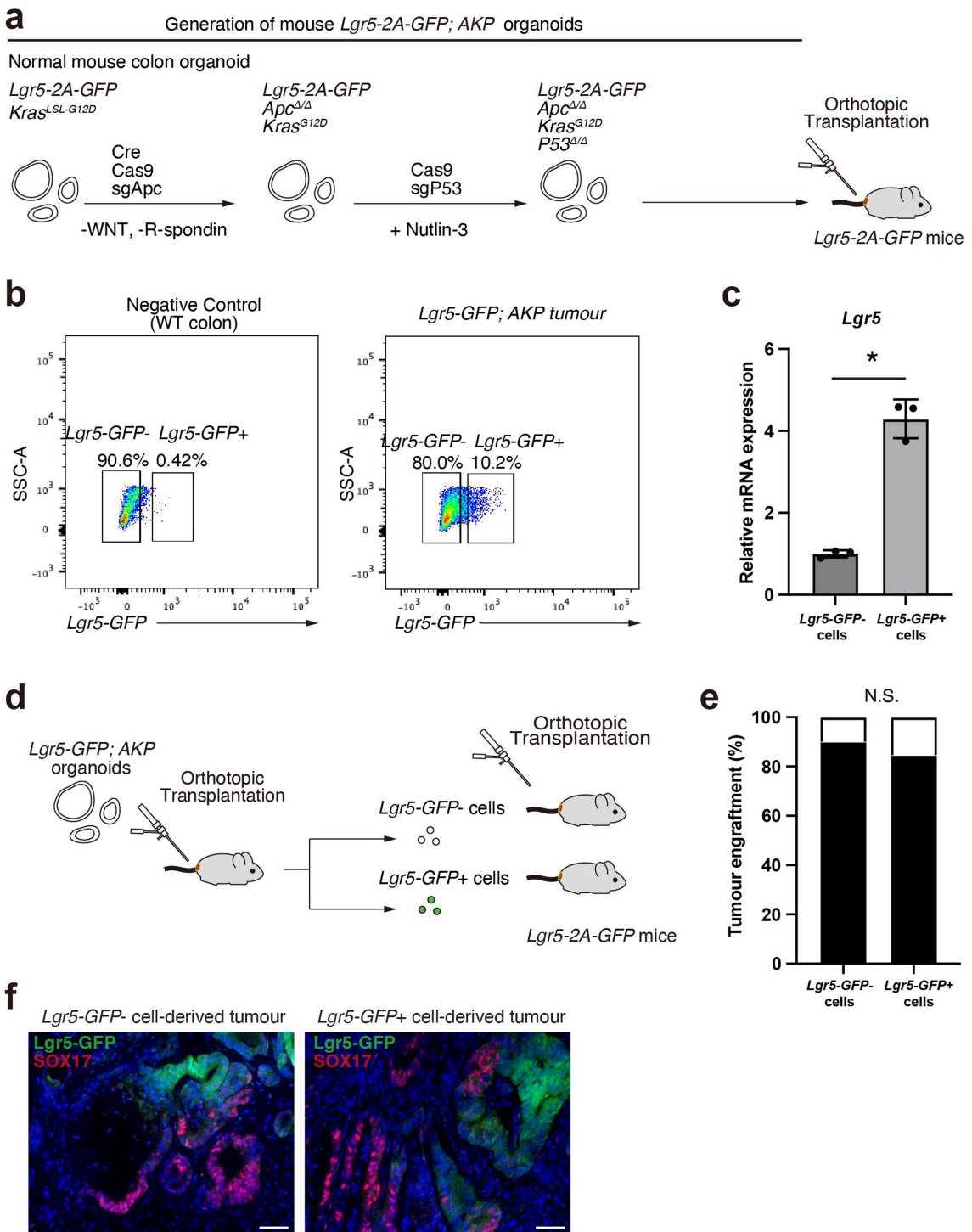
tumours versus SOX17^{low/neg} tumours. n = 39 cases. Tumours were classified into SOX17^{high} ($\geq 70\%$), SOX17^{med} ($< 70\%, \geq 30\%$), SOX17^{low} ($< 30\%, > 0\%$), and SOX17^{neg} (0%) based on the percentage of SOX17 nuclear staining-positive cells. Tumours with ≥ 50 CD8+ cells per x20 field were classified as CD8^{high} tumours, < 50 CD8+ cells per x20 field as CD8^{low} tumours. Scale bar, 20 μ m (a, c). Fisher's exact test (e). *p < 0.05.

a**b****c****d****e****f****g****h****i**

Extended Data Fig. 13 | Frequency of Lgr5-GFP⁺ cells decreases over time in adenomas. **a**, Schematic of time-course analysis of the tumours in *Lgr5-CreERT2; Apc f/f* mice after tamoxifen injections. **b, c**, IF for *Lgr5-GFP* and β -catenin in *Lgr5-CreERT2; Apc f/f* mouse intestines (**b**) and quantification for the percentage of *Lgr5-GFP*⁺ cells in β -catenin nuclear accumulation positive tumour cells (**c**). n = 30 fields from 5 mice per group. **d**, Schematic of anti-CD8 antibody treatment in *Lgr5-CreERT2; Apc f/f* mice with tamoxifen injections. **e, f**, IF for *Lgr5-GFP* (**e**) and quantification of *Lgr5-GFP*⁺ areas (**f**) in anti-CD8 or isotype antibody-treated

Lgr5-CreERT2; Apc f/f mouse intestines. n = 10 fields from 5 mice per group. **g**, *Lgr5* mRNA expression in RNA-seq of control and SOX17KO AKP organoids. n = 3 per group. **h**, ISH for *Lgr5* in control and SOX17OE AKP tumours. Representative of n = 9–11 mice per group. **i**, qRT-PCR for *Lgr5* mRNA expression in control and SOX17OE naïve AKP organoids. n = 3 per group. One-way ANOVA (**c**). Unpaired two-tailed t-test (**f, g, i**). Data are mean \pm SEM (**c**) and mean \pm SD (**f, g, i**). *p < 0.05. Scale bar, 50 μ m (**b, e**), 20 μ m (**h**).

Article



Extended Data Fig. 14 | LGR5⁺ and LGR5⁻ tumour cells are highly plastic and give rise to one another during tumour growth. **a**, Schematic of generation of *Lgr5-GFP; AKP* organoids and orthotopic transplantation. **b**, Flow cytometry for *Lgr5-GFP*⁺ cells from *Lgr5-GFP; AKP* tumours and wild-type colon epithelia (negative control). Representative of $n = 6$ mice. **c**, qRT-PCR for *Lgr5* mRNA expression in sorted *Lgr5-GFP*⁻ and *Lgr5-GFP*⁺ cells from *Lgr5-GFP; AKP* tumours. $n = 3$ mice per group. **d, e**, Schematic (**d**) and tumour engraftment rate (**e**) of

orthotopic transplantation of sorted *Lgr5-GFP*⁻ and *Lgr5-GFP*⁺ cells into the colons of immunocompetent mice. In each mouse, 4,000 cells were orthotopically transplanted. $n = 10$ –13 mice per group. Representative of two independent experiments. **f**, IF for *Lgr5-GFP* and *SOX17* in *Lgr5-GFP*⁻ cell-derived tumours and *Lgr5-GFP*⁺ cell-derived tumours. Representative of $n = 6$ mice per each group. Unpaired two-tailed t-test (**c**). Fisher's exact test (**e**). Data are mean \pm SD. N.S. not significant. * $p < 0.05$. Scale bar, 50 μ m (**f**).

Reporting Summary

Nature Portfolio wishes to improve the reproducibility of the work that we publish. This form provides structure for consistency and transparency in reporting. For further information on Nature Portfolio policies, see our [Editorial Policies](#) and the [Editorial Policy Checklist](#).

Statistics

For all statistical analyses, confirm that the following items are present in the figure legend, table legend, main text, or Methods section.

n/a Confirmed

- The exact sample size (n) for each experimental group/condition, given as a discrete number and unit of measurement
- A statement on whether measurements were taken from distinct samples or whether the same sample was measured repeatedly
- The statistical test(s) used AND whether they are one- or two-sided
Only common tests should be described solely by name; describe more complex techniques in the Methods section.
- A description of all covariates tested
- A description of any assumptions or corrections, such as tests of normality and adjustment for multiple comparisons
- A full description of the statistical parameters including central tendency (e.g. means) or other basic estimates (e.g. regression coefficient) AND variation (e.g. standard deviation) or associated estimates of uncertainty (e.g. confidence intervals)
- For null hypothesis testing, the test statistic (e.g. F , t , r) with confidence intervals, effect sizes, degrees of freedom and P value noted
Give P values as exact values whenever suitable.
- For Bayesian analysis, information on the choice of priors and Markov chain Monte Carlo settings
- For hierarchical and complex designs, identification of the appropriate level for tests and full reporting of outcomes
- Estimates of effect sizes (e.g. Cohen's d , Pearson's r), indicating how they were calculated

Our web collection on [statistics for biologists](#) contains articles on many of the points above.

Software and code

Policy information about [availability of computer code](#)

Data collection

Flow cytometry data were collected using FACSDiva software (version 8.0, BD Biosciences).

Images of immunofluorescence were acquired using a Nikon Eclipse 90i upright microscope equipped with a Hamamatsu Orca-ER CCD camera, and APC line 1200 light source.

Data analysis

Flow cytometry data were analyzed using FlowJo software (version 10, TreeStar).

Statistical analysis was performed by GraphPad Prism 9.3.1.

ImageJ v2.1.0/1.53c was used for the quantification of fluorescent area in the images

For manuscripts utilizing custom algorithms or software that are central to the research but not yet described in published literature, software must be made available to editors and reviewers. We strongly encourage code deposition in a community repository (e.g. GitHub). See the Nature Portfolio [guidelines for submitting code & software](#) for further information.

Data

Policy information about [availability of data](#)

All manuscripts must include a [data availability statement](#). This statement should provide the following information, where applicable:

- Accession codes, unique identifiers, or web links for publicly available datasets
- A description of any restrictions on data availability
- For clinical datasets or third party data, please ensure that the statement adheres to our [policy](#)

Bulk RNA-seq data, ATAC-seq data, and single-cell RNA-seq data have been deposited at GEO (accession number: GSE222713)

Human research participants

Policy information about [studies involving human research participants](#) and [Sex and Gender in Research](#).

Reporting on sex and gender

Resected human colonic sections that were diagnosed as adenomas were obtained from 8 patients with familial adenomatous polyposis (FAP) and 11 patients without FAP. Resected human colonic sections that were diagnosed as CRCs at different pathologic tumour stages (pT1-pT4) were obtained from 39 patients. Inclusion criteria were male or female adults aged 20–90 years.

Population characteristics

Inclusion criteria were male or female adults aged 20–90 years.

Recruitment

Resected human colonic sections that were diagnosed as adenomas were obtained from 8 patients with familial adenomatous polyposis (FAP) and 11 patients without FAP. Resected human colonic sections that were diagnosed as CRCs at different pathologic tumour stages (pT1-pT4) were obtained from 39 patients.

Ethics oversight

The Massachusetts General Hospital (MGH) Institutional Review Board committee approved the study protocol.

Note that full information on the approval of the study protocol must also be provided in the manuscript.

Field-specific reporting

Please select the one below that is the best fit for your research. If you are not sure, read the appropriate sections before making your selection.

Life sciences Behavioural & social sciences Ecological, evolutionary & environmental sciences

For a reference copy of the document with all sections, see nature.com/documents/nr-reporting-summary-flat.pdf

Life sciences study design

All studies must disclose on these points even when the disclosure is negative.

Sample size

No statistical methods were used to predetermine sample size. Sample sizes were based on those used in previous and preliminary studies from our lab.

Data exclusions

For the single-cell RNA-seq data, doublets and cells with low mRNA quality were discarded as described in the method section.

Replication

All experiments presented in this study were performed using at least 3 biological replicates. All presented results were repeatable.

Randomization

Mice were allocated to study groups randomly.

Blinding

Blinding was not performed in the experiments.

Reporting for specific materials, systems and methods

We require information from authors about some types of materials, experimental systems and methods used in many studies. Here, indicate whether each material, system or method listed is relevant to your study. If you are not sure if a list item applies to your research, read the appropriate section before selecting a response.

Materials & experimental systems

n/a	Involved in the study
<input type="checkbox"/>	<input checked="" type="checkbox"/> Antibodies
<input type="checkbox"/>	<input checked="" type="checkbox"/> Eukaryotic cell lines
<input checked="" type="checkbox"/>	<input type="checkbox"/> Palaeontology and archaeology
<input type="checkbox"/>	<input checked="" type="checkbox"/> Animals and other organisms
<input checked="" type="checkbox"/>	<input type="checkbox"/> Clinical data
<input checked="" type="checkbox"/>	<input type="checkbox"/> Dual use research of concern

Methods

n/a	Involved in the study
<input checked="" type="checkbox"/>	<input type="checkbox"/> ChIP-seq
<input type="checkbox"/>	<input checked="" type="checkbox"/> Flow cytometry
<input checked="" type="checkbox"/>	<input type="checkbox"/> MRI-based neuroimaging

Antibodies

Antibodies used

IHC:
 goat polyclonal anti-SOX17 (1:200, R&D, AF1924)
 rabbit monoclonal anti-SOX17 (1:2000, abcam, ab224637)
 rabbit monoclonal anti-CD4 (1:400, abcam, ab183685)
 rabbit monoclonal anti-CD8 (1:1000, abcam, ab217344).
 mouse monoclonal anti-β-catenin (1:50, BD Biosciences, 610154)
 rat monoclonal anti-BrdU (1:2000, abcam, ab6326)
 mouse monoclonal anti-Ki67 (1:400, BD, 550609)
 mouse monoclonal anti-CD8 (1/100, Abcam, ab17147)

IF:
 rabbit monoclonal anti-Phospho-Stat1 (1:400, Cell signaling, #9167)
 rabbit monoclonal anti-SOX17 (1:2000, abcam, ab224637)
 goat polyclonal anti-GFP (1:500, abcam, ab6673)

Flow cytometry:
 CD45 APC (1:200, Biolegend, 103112)
 EpCAM eFluor450 (1:50, Thermo Fisher Scientific, 48-5791-82)
 MHC-I eFluor450 (1:100, Thermo Fisher Scientific, 48-5958-82)
 CD8a BUV395 (1:400, BD, 563786)
 IFNg FITC (1:200, Biolegend, 505806)
 TNFa PE (1:400, Biolegend, 506306)
 IFNAR-1 (1:00, Biolegend, 127305)
 CD119 (IFN-γ R α chain) (1:200, Biolegend, 112803)
 APC streptavidin (1:200, Biolegend, 405207)

In vivo dosing:
 CD8α antibody (BioXcell, BE0061)
 CD4 antibody (BioXcell, BE0003-1)
 IgG isotype antibody (BioXcell, BE0090)
 IFNAR1 antibody (BioXcell, BE0241)
 IFNγ antibody (BioXcell, BE0055)
 IgG1 isotype antibody (BioXcell, BE0083)

Validation

All antibodies for IHC, IF, flow cytometry, and in vivo dosing were well-recognized clones in the field and validated by the manufacturers.

Eukaryotic cell lines

Policy information about [cell lines](#) and [Sex and Gender in Research](#)

Cell line source(s)

Organoid lines were developed by the authors from normal colon crypts from mice and human.

Authentication

Authentication of genetic events were confirmed as described in the manuscript.

Mycoplasma contamination

Organoid lines have been routinely tested and confirmed negative for mycoplasma contamination.

Commonly misidentified lines (See [ICLAC](#) register)

None

Animals and other research organisms

Policy information about [studies involving animals](#); [ARRIVE guidelines](#) recommended for reporting animal research, and [Sex and Gender in Research](#)

Laboratory animals

Both male and female mice were used at the ages of 8-12 wks.

Wild animals	Wild animals were not used in this study.
Reporting on sex	Both male and female mice were used at the ages of 8-12 wks.
Field-collected samples	This study did not involve samples collected in the field
Ethics oversight	Mice were under the husbandry care of the Department of Comparative Medicine in the Koch Institute for Integrative Cancer Research. All procedures were conducted in accordance with the American Association for Accreditation of Laboratory Animal Care and approved by MIT's Committee on Animal Care.

Note that full information on the approval of the study protocol must also be provided in the manuscript.

Flow Cytometry

Plots

Confirm that:

- The axis labels state the marker and fluorochrome used (e.g. CD4-FITC).
- The axis scales are clearly visible. Include numbers along axes only for bottom left plot of group (a 'group' is an analysis of identical markers).
- All plots are contour plots with outliers or pseudocolor plots.
- A numerical value for number of cells or percentage (with statistics) is provided.

Methodology

Sample preparation

Details are described in the method section. Briefly, colon tumours were collected, minced, and digested in a digestion buffer. Tumours were then further dissociated with a gentleMACS Octo Dissociator, filtered through a 100-µM filter, and centrifuged for 5 min at 2000 rpm. To isolate lymphocytes, cells were resuspended in 5 ml 44% percoll, underlaid with 2ml 67% percoll, centrifuged at 2000 rpm for 20 min with no brake. Buffy coat at the interface was isolated, resuspended in culture media, and centrifuged at 2000 rpm for 10 min.

Instrument

BD LSRFortessa four-laser, 18-color flow cytometer and FACS Aria II were used.

Software

FACSDiva software (version 8.0, BD Biosciences) and FlowJo software (version 10, TreeStar).

Cell population abundance

When CD45+ cells were sorted for scRNA-seq , the purity was confirmed by UMAP plot with Ptprc expression.

Gating strategy

Single lymphocytes were gated on FSC-A versus SSC-A, FSC-H versus FSC-W, and SSC-H versus SSC-W. Live CD8+ T cells were gated on positive CD8α and negative Fixable Viability Dye eFluor™ 780 staining. For scRNA-seq, CD45+ immune cells were gated on negative 7-AAD, negative EpCAM, and positive CD45 staining.

Tick this box to confirm that a figure exemplifying the gating strategy is provided in the Supplementary Information.